NUMERICAL ANALYSIS OF FLUID DYNAMICS AND SOLIDS CONTACT MECHANISMS IN HUMAN TRACHEA UNDER MECHANICAL VENTILATION FOR ENDOTRACHEAL CUFF DESIGN

ALEJANDRA HERNÁNDEZ ESCOBAR

UNIVERSIDAD EAFIT
ESCUELA DE INGENIERÍAS, UNIVERSIDAD EAFIT
MAESTRÍA EN INGENIERÍA
MEDELLÍN
2021

NUMERICAL ANALYSIS OF FLUID DYNAMICS AND SOLIDS CONTACT MECHANISMS IN HUMAN TRACHEA UNDER MECHANICAL VENTILATION FOR ENDOTRACHEAL CUFF DESIGN

ALEJANDRA HERNÁNDEZ ESCOBAR

Trabajo de grado para optar al título de Magíster en Ingeniería

Advisor(s)
Raúl A. Valencia, Ph.D.

UNIVERSIDAD EAFIT
ESCUELA DE INGENIERÍAS, UNIVERSIDAD EAFIT
MAESTRÍA EN INGENIERÍA
MEDELLÍN
2021

Nota de aceptación

Firma
Nombre:
Presidente del jurado

Firma
Nombre:
Jurado

Firma
Nombre:
Jurado

Medellín, August 12, 2021

Acknowledgements

The author thanks the school of engineering of the EAFIT University for their support on the development of this project.

This research was only possible to be developed with the help of Raúl A. Valencia Cardona, promoter of this thesis; and Juan D. Gómez Cataño, adviser and main professor of the master courses. My deepest appreciation towards them, for enriching this project with scientific knowledge, guidance, and encouragement.

Sincere thanks to Marco A. González Agudelo, MD., principal interested in the development of this work, as the incredible doctor and researcher he is. Without his cooperation and expertise the project would have never started, less alone come to an end.

Special mention and admiration towards Philip Cardiff,PhD., principal developer of Solids4foam, who selflessly replied to my messages when having trouble with the tool's implementation and understanding.

Finally, the author wishes to express immense gratitude towards family and friends for being always present, supporting and believing in this project and in the curious person behind it. This thesis is dedicated to you all.

Resumen

Este proyecto tiene como objetivo aportar una nueva perspectiva a la línea de investigación en aplicaciones biomédicas y de bioingeniería, particularmente la línea de dispositivos biomédicos. Esto se logrará mediante el análisis de algunos parámetros en modelos idealizados de vías respiratorias humanas para contribuir al proceso de diseño de un neumotaponador endotraqueal. Este dispositivo juega un papel fundamental en el proceso de ventilación mecánica cuando se utiliza un tubo endotraqueal. Su función es asegurar un sellado correcto al final de la tráquea, para evitar la filtración de partículas a los pulmones, minimizando así la posibilidad de desarrollar neumonía. También es fundamental evaluar cómo interactúa el dispositivo con el flujo de aire y la pared traqueal, ya que una lesión en esa zona debido a tensiones elevadas es, desde todos los puntos de vista, indeseable. La investigación propuesta incluye dos frentes de trabajo, primero, el análisis del comportamiento fluido-dinámico en la tráquea mediante la implementación de simulaciones numéricas en estado estacionario y transitorio, con el fin de evaluar cómo los cambios en el dominio computacional y modelos de turbulencia afectan los resultados; en segundo lugar, la propuesta de una metodología para análisis del comportamiento estructural en geometrías idealizadas por medio del método de volúmenes finitos en la herramienta de software libre "solids4Foam". Éste trabajo está enmarcado en un proyecto de la convocatoria de proyectos conjuntos de I+D+i, en el marco de la agenda regional 2020 titulada: "Desarrollo y validación de un nuevo diseño de neumotaponador integrado a un tubo orotraqueal que permita la prevención de la neumonía asociada a la ventilación mecánica en pacientes de cuidado intensivo". De manera que la presente investigación pretende constituir una primera aproximación que permita a los investigadores evaluar y concluir hacia la meta final de un diseño de neumotaponador endotraqueal satisfactorio y su relevancia para evitar efectos indeseables en pacientes ventilados mecánicamente.

PALABRAS CLAVE:

Sistema respiratorio superior, Modelacón de contacto entre sólidos, Dinámica de fluidos computacional, Ventilación Mecánica, Método de volúmenes finitos, Neumotaponador Orotraqueal.

Abstract

This project aims to bring a new perspective to the line of research in biomedical and bioengineering applications, particularly the line of biomedical devices. This is to be achieved by analyzing some parameters on in idealized models of human airways to contribute to the design process of an endotracheal cuff. This device plays a fundamental role in the mechanical ventilation process when using an endotracheal tube. Moreover, its function is to ensure a proper seal at the end of the trachea, to avoid particle filtration to the lungs, avoiding in this way the possibility to develop pneumonia. It is also paramount to evaluate how the device interacts with the airflow and the tracheal wall since a lesion on that area due to high stresses is, from all points of view, undesirable. The proposed research includes two work fronts, first, the analysis of fluid-dynamic behavior in the trachea through the implementation of numerical simulations in steady and transient state, in order to evaluate how changes in the computational domain and turbulence models affect the results; secondly, the proposal of a methodology for the analysis of the structural behavior in idealized geometries by means of the finite volumes method in the free software tool “ solids4Foam ”. This work is framed in a project of the call for joint I + D + i projects, within the framework of the 2020 regional agenda entitled: “ Development and validation of a new design of a pneumatic cuff integrated to an orotracheal tube that allows prevention of ventilator-associated pneumonia in intensive care patients ”. Thus, the present research aims to constitute a first approach that allows researchers to evaluate and conclude towards the final goal of a successful endotracheal pneumo-cuff design and its relevance to avoid undesirable effects in mechanically ventilated patients.

KEYWORDS:

Human Upper Airway (HUA), Structural contact modeling, Computational Fluid Dynamics

(CFD), Mechanical Ventilation, Finite Volume Method (FVM), Endotracheal Cuff.

Contents

List of Figures

List of Tables

Pag.

Chapter 1

Introduction

1.1 MOTIVATION

The project is outlined in the biomedical devices research line, since the aim is to evaluate, from the computational point of view, the fluid-dynamic behavior on the trachea, and the structural conduct of an idealized version of a pneumo-cuff; to contribute on a bigger research focused on developing new designs for this device. This pursue is based on the idea of minimizing pneumonia decease, frequently encountered on mechanically ventilated patients.

The research puts the department of Antioquia, Colombia, as the epicenter in this regard, through the development and analysis of new designs for the endotracheal cuff, given that one of the purposes is to obtain scientific knowledge that can translate into useful insights for the specialized medical practitioners through comprehensive research. That will be possible thanks to the integration of different resources and actors: EAFIT University for the numerical simulations here proposed, the SENA institute coupled with the Universidad de Antioquia, working on synthesis between nano-particles with antibacterial functions, and CES University regarding in vivo and in vitro experiments.

This conversion from scientific knowledge to applicable conclusions and even prototype development comes as a solution. The last affirmation since the project arises from the Doctoral Thesis of Dr. Marco A. González Agudelo, who developed enough research, criteria, and experience to be able to relate pneumonia disease with the mechanical ventilation process, more specifically, due to the selection of the adequate endotracheal tube and respective cuff. Furthermore, the literature suggests that most research conducted applying numerical studies to the respiratory system were related to human upper airway (HUA) simulations that considerably focused on the aspects of fluid dynamics and airflow patterns. However, there is a literature gap in obtaining information on the effects of fluid-structure interaction (FSI), especially on simulations considering a foreign object, as the endotracheal tube would be. Then, the results from this project will be helpful to the adequate development of the mentioned doctoral thesis, as well as for the rest of the medical community and the medical supplies industry.

This work is related to the applied sciences field, which is one of the emphases of the Master Course in Engineering of EAFIT University. This program provides the theoretical frame for any application on which numerical simulations are to be performed, based on the continuum mechanics principles. Here, the fundamentals of fluid and solid mechanics are analyzed, taking advantage of various numerical approaches. Moreover, a variety of experiments are to be conducted according to the scientific nature of the problem. With this, it becomes possible to obtain experimental data to validate the computations.

1.2 PROBLEM STATEMENT

30 to 50% of the patients admitted to an ICU require ventilatory support due to their pulmonary pathology (Esteban et al., 2013). Ventilation-associated pneumonia (VAP) is an infection mainly associated with intensive care unit care and occurs in between 10% and 60% of intubated patients (Nair & Niederman, 2015; Pneumatikos, Dragoumanis, Bouros, Warner, & Warner, 2009). In Colombia, according to 2018 data published by the National Institute of Health, the incidence of VAP was 28.4%, and in Antioquia, according to the epidemiological report of the Sectional Health Directorate, it was 26.56%, very similar to those reported in developed countries. The mortality attributable to VAP is 30%, and it contributes to the death between 50% and 70% of patients admitted to the ICU (Nair & Niederman, 2015; Pneumatikos et al., 2009). VAP contributes to an increase in the days of hospitalization in the ICU, requires treatment with antibiotics for 7 to 15 days, with consequences in adverse effects and generation of bacterial resistance (Nair & Niederman, 2015; Pneumatikos et al., 2009). The cost of NAV in the United States is $10,000 to $25,000 per case (Papazian, Klompas, & Luyt, 2020). In Colombia, the values reported by a study carried out in the city of Cartagena was $44,354 per patient, compared with $5,037 in those who do not present this infection.

The main risk factor for VAP is the orotracheal tube, which increases the risk factor between 6 to 21 times by decreasing the mucociliary function of the respiratory tract, altering the cough reflex and promoting the accumulation of tracheobronchial secretion above the pneumatic cuff and facilitate micro-aspiration of bacteria accumulated on the walls of the material. (Papazian et al., 2020; Pneumatikos et al., 2009) Many efforts have been made to avoid micro-aspiration in intubated patients, investigating the architecture of the orotracheal tubes, different materials, changes in the shape of the pneumatic cuff, variation of the pressure and volume of the pneumatic cuff, sealing over tracheal mucosa, impregnation of the wall of the orotracheal tube with antimicrobials, and the combination of several of these mechanisms. (Fernandez, Levine, & Restrepo, 2012; Jaillette et al., 2017). There is currently no ideal tube that prevents micro-aspiration and bio-film formation as the main accepted mechanisms in the pathophysiology of VAP.

The objective of this project is to develop and validate a new design of a pneumatic cuff integrated into an orotracheal tube employing numerical simulations and experimental procedures, aiming at the reduction of micro-aspiration for the prevention of pneumonia associated with mechanical ventilation. This proposal seeks to join efforts to reduce the risk of VAP in patients with mechanical ventilation, reduce health care costs, and allow rapid and functional recovery of the patient admitted to the ICU.

1.3 JUSTIFICATION

Pneumonia related to the endotracheal tube is caused by inspiration when the secretion colonized by bacteria accumulated in the upper part of the endotracheal cuff is filtered through the walls of the endotracheal tube, migrating into the bronchial tree and reaching the pulmonary alveolus, where it reacts with alveolar macrophages producing the pneumonic picture. Multiple actions have been carried out to prevent VAP in intubated patients, modifying designs of endotracheal tubes and cuff, introducing changes in materials and physical conditions such as the pressure on the cuff, adding suction channels to aspirate tracheal secretion, among others. However, there is currently no ideal tube that prevents micro-aspiration and biofilm formation, which are the main accepted mechanisms for VAP production. The objective of this project is to take advantage of numerical methods of applied sciences and experimental procedures to develop and validate a new design of a pneumatic cuff with a geometric configuration that enables the reduction of microaspiration by bacteria for the prevention of ventilation-associated pneumonia mechanics.

1.4 KEY CONCEPTS

1.4.1 PATHOPHYSIOLOGY OF VENTILATOR-ASSOCIATED PNEUMONIA

Ventilator-associated pneumonia (VAP) occurs in between 10% and 60% of patients on ventilatory support with a mechanical ventilator, and mortality from this care-associated infection is 30%. The most widely accepted theory about the pathophysiology of pneumonia in these patients is bronchial aspiration (Blot, Poelaert, & Kollef, 2014; Nair & Niederman, 2015; Pneumatikos et al., 2009). The orotracheal tube (TOT) has a built-in cuff that, when inflated with air, makes a seal with the wall of the trachea; such inflation should not generate a pressure greater than 30 cm $H2O$ to avoid ischemic damage to tracheal cells by compression. When producing the seal, the pneumatic cuff accumulates on its upper external surface, salivary secretions that come from the oral cavity and secretions due to regurgitation of gastric fluid from the digestive tract; These fluids are conducive to bacterial growth that can migrate through the space between the biomaterial of the cuff and the wall of the trachea (Rosero, Ozayar, Eslava Schmalbach, Minhajuddin, & Joshi, 2018; RouzÃ©, Jaillette, Poissy, PrÃ©au, & Nseir, 2017; Spapen et al., 2017). Several studies have shown that the bacteria isolated from orotracheal secretions are the same as those recovered from lung tissue in patients with pneumonia and mechanical ventilation. Several studies have been carried out with different methodologies to determine the route of entry of these secretions to the lung, showing that the secretions pass through a virtual space between the outer layer of the cuff's material and the inner wall of the trachea (Lorente, Lecuona, JimÃ©nez, Mora, & Sierra, 2007; Muscedere et al., 2011; Papazian et al., 2020). To avoid microaspiration, researchers have focused on the characteristics of the endotracheal cuff in terms of their material, shape, volumetric capacity, and pressure generation (Fernandez et al., 2012; Li Bassi et al., 2015).

Evolution of the orotracheal tubes The first orotracheal tube studied was constructed from polyvinylchloride (PVC) with a cuff that had a limited container and generated high pressures when inflated. Its shape when inflated was round and generated enough pressure to maintain a seal without allowing air leakage and in theory neither slipping of the secretion accumulated on top of the cuff; However, the pressure of the same was higher than the perfusion pressure of the tracheal tissue, producing an ischemic injury that led to damage to the trachea with consequences of necrosis and stenosis due to poor healing (RouzÃ© et al., 2017). Subsequently, by inverting the reasoning behind the previously mentioned endotracheal tube, the design of the pneumatic cuff was improved, achieving a greater contact area with the trachea in such a way that, to be filled, it required more air volume and generated less pressure, thus solving the effect on the perfusion of the cuff of the previous device. The pressure of the cuff had to be maintained at a maximum of $30cmH2O$ to avoid ischemia of the tissue and to allow perfusion pressure in the tracheal tissue; this pressure oscillated with the pressure changes of the respiratory cycle, allowing the secretion to pass through the cuff without ensuring a constant seal. The material used was the same as the previously mentioned tube; however, it was evident that due to the thickness of its outer layer, the material folded back, generating channels through which secretions slid into the bronchial lumen due to gravity. (Jaillette et al., 2017; Spapen et al., 2017).

The polyurethane was then evaluated as a material to make the cuff for being thinner, mechanically resistant, and easy to handle. This made it possible to change the shape when it was inflated, going from a cylindrical to a conical shape, achieving a better seal in the upper part with the trachea and avoiding the folds that were given with the PVC cuffs, thus reducing the passage of secretion around the cuff ("Guidelines for the management of adults with hospital-acquired, ventilator-associated, and healthcare-associated pneumonia.", 2005; Lorente et al., 2007). The TOT with a polyurethane cap is the most used today. Studies continue to show that, although PVC endotracheal tubes continue to present microaspiration and VAP, then the problem of microaspiration has not been solved. For this reason, there was a new development in the orotracheal tubes, which consisted of incorporating a continuous suction system to avoid the accumulation of secretions above the upper surface of the cuff. Several studies and a meta-analysis have been published analyzing this new orotracheal tube, yielding favorable results in terms of reducing the number of days of mechanical ventilation; however, the number of VAP episodes seems not to reduce but its appearance delayed, that is, appears after the second week of being supported with a mechanical ventilator. Another technology incorporated in the TOT is a device that allows to measure and maintain the pressure of the cuff to control the sealing and perfusion in the trachea, but not positive results were shown, nor was it evidenced if there are adverse events such as findings of tracheal injuries (Blot, Rello, & Koulenti, 2016; Dave, Frotzler, & Weiss, 2011; Jaillette et al., 2017; Lorente et al., 2007; Muscedere et al., 2011; Philippart et al., 2015; Suhas, Kundra, & Cherian, 2016; Valencia et al., 2007; Weiss et al., 2009). Furthermore, endotracheal tubes have been designed with combinations of micro-aspiration prevention mechanisms, such as the PneuX, which has a polyurethane cuff that does not allow kinks, is of high volume and low-pressure type, demonstrating a decrease in secretion leakage through the wall of the cuff, while maintaining the pressure of the same and compensation with PEEP. This research aims to design an orotracheal cuff of geometry and material that beyond doubt prevents micro-aspiration of the secretion accumulated in the airway, thus impact on reducing or avoiding VAP, avoiding associated mortality and costs generated in the care of critical patients.

1.5 OBJECTIVES

The purpose of this research project is to evaluate idealized models of the human upper airway and endotracheal cuff. The goal is to investigate changes in various parameters such as the geometrical and turbulence models used for the viscous-flow simulations, as well as possible modifications in the tracheal wall in terms of stresses and strains due to the structural contact between the pneumo-cuff and the air-wall involved on the mechanical ventilation phenomena.

1.5.1 GENERAL

Analyze fluid dynamics and solids contact on simplified upper airway and endotracheal cuff models, through numerical simulations and methodology establishment when using the finite volume method; as well as a decent state of the art focused on relevant numerical simulations attempting to understand the human breathing process and deceases linked to it. This with the aim of bring some practical implications when future researchers ge to the task of innovating the endotracheal cuff design to avoid pneumonia disease on mechanically ventilated patients.

1.5.2 SPECIFIC

- Develop a brief state of the art on numerical researches working on the breathing phenomena simulation from three points of view: fluid-dynamic behavior, particle transport or deposition, and fluid-structure interaction.
- Develop a brief state of the art on numerical researches working on the breathing phenomena simulation from three points of view: fluid-dynamic behavior, particle transport or deposition, and fluid-structure interaction.Analyze fluid dynamic behavior, by means of numerical implementations, on both idealized and realistic models of the HUA of an adult patient when varying turbulence models and time discretization schemes on three-dimensional models.
- Formulate a model and its methodology for structural behavior analysis, specifically for solids contact problems, using the finite volume method on OpenFOAM's environment through the solids4Foam toolkit.

1.6 THESIS ORGANIZATION

This thesis brings together ideas from fluid dynamics, solid mechanics, and the use of open-source toolkit solids4Foam. With these tools in hand, the thesis proposes means to study and analyze first, fluid dynamic behavior on two different geometry models that attempt to simulate a human trachea; when proposing also various turbulence models. Second, a solids contact methodology is performed under the same finite volume method to bring to the table the concern about how the trachea may deform when a patient is submitted to mechanical ventilation. The analyses are meant to give some insight (a first approximation, if you'd like), to understand how these factors (different geometries, turbulence models, FVM approximations to solid mechanics) intervene in obtaining accurate results when comparing them with other researches; having in mind that the computational science has become in the last century a powerful ally for biomedical procedures and investigation. The theme is in nature for someone who has a background in continuum mechanics, OpenFOAM's environment, some medical interest, and feels fine reading the language that is math. Acknowledging that in general it is not very common to find someone that feels comfortable around all the aforementioned topics, this book is written to cover the basic tools for understanding the whole matter. Because of this and since the thesis covers various topics, the text is rather long; consequently, the author appeals to the reader's patience. The description of the thesis organization herein looks forward to informing the reader about what to find where and allow each person to adjust to their interests.

The book is divided into three parts that follow this introductory chapter: (I) Basics, (II) Numerical Simulations, and (III) Epilogue. Part I, *Basics*, contains one chapter that intends to briefly introduce the work done by previous researchers to numerically simulate fluid dynamics, particle deposition and fluid-structure interaction in human upper airways.

Part II, is comprised of Chapter 3 and 4. The third chapter deals with the computational or numerical aspect of the fluid dynamics involved in the breathing process, and viscous-flow computations with different variables are carried out and discussed. Chapter 4 deals with basic approximations of solid mechanics, more specifically solid's contact under the finite volume approach with the solids4Foam tool.

Part III, encompasses Chapter 5, that brings commonplace Conclusions and Further Work that intend to wrap-up the main purpose of this thesis: brief analyses of the implications that the use of numerical simulations has when aiming to gain some engineering insight on biomedical phenomena, taking into consideration quasi-static and transient approaches and the assembly of various tools to investigate on the mechanical ventilation subject. As the reader will find, Chapter 6 contains an Annex that tries in contributing to the understanding of the theory behind the fluid-structure mathematical formulation, topic that is relevant to accurately describe more "realistic" breathing processes. The book ends up with Appendix A on turbulence modeling used for viscous-flow computations, and Appendix B on the step-by-step explanation on the solids4Foam architecture and commands used for the solids contact analyses. At the very end, References, without whom the author would never have been able to advance on this project.

Part I

Basics

Chapter 2

State of the art

As pointed out by Wall and Rabczuk (2008), airflow in the lung is of high interest in pulmonary medicine. For example, airflow patterns and the resulting particle and aerosol depositions play a key role in the pharmaceutic industry. They are also of interest in intensive-care medicine when patients have to be mechanically ventilated, as it is the case of this research. Related topics have been widely investigated by many researchers covering various aspects, however, we are particularly interested in airflow patterns, particle deposition phenomena, and stress distributions in airway walls of mechanically ventilated patients in order to assess the design for an endotracheal cuff. Therefore, the main objective of this section is to shortly review the literature that proposes different numerical approaches that could help on that endeavor.

2.1 FLUID DYNAMICS AND FLOW PATTERNS

The research reported on this section includes the use of the Navier-Stokes equations via *computational fluid dynamics* (CFD) to help visualize the actual mechanism of the airflow to assist in making strategic and reasonable decisions regarding the adoption of treatment methods in clinical settings. Doorly, Taylor, and Schroter (2008) reviewed the mechanics of airflow in the human nasal airways, drawing on the findings of experimental and computational model studies. The processes entailed in modeling the nasal airways (from defining the model, to its production and, finally, validating the results) was critically examined on this study, both for physical models and for computational simulations. They conclude there is considerable work to be done in the area of rational geometry characterization, which should aim to provide the ability to describe both model and real, subject-specific, normal and pathological geometries objectively and comparatively. Later on, Faizal et al. (2020)presented a review article on which they found that the *human upper airway* (HUA) has been well studied through the application of CFD, which had considerably enhanced the understanding of flow in HUA. In addition, the article summarizes the review in the form of method of studying the HUA, CFD approach, and the application of CFD for predicting HUA obstacle, including the type of CFD commercial software are used in this research area. They also found that most studies have focused on the pollutant transport and drug delivery in respiratory systems, whereas others focused on sleep-disordered breathing.

Phuong and Ito (2015) investigated the flow pattern in HUA including oral and nasal inhalation in a realistic replica model of the human respiratory tract. Experimental and numerical methods were used; *particle image velocimetry* (PIV) was performed under three constant breathing conditions; furthermore, CFD analyzes were conducted on four turbulence models with boundary conditions corresponding to the experimental models. They found the flow field at the higher flow rate to be very challenging for some turbulence models. In addition, the geometry is highly curved in many regions as this research includes the nasal/oral cavity, pharynx, larynx and trachea. Geometry changes causes the flow pattern to increase in complexity which could result in significant anisotropic turbulence, being that a limitation of the turbulence models used in this research. The study performed by X. Xu, Wu, Weng, and Fu (2020) is very similar, in the sense that they also combined the PIV-CFD approach to study the flow field characteristics in the trachea region, under three constant inhalation and exhalation conditions. Here, the effects of flow rates and breathing modes on the airflow patterns were investigated. They affirm that the turbulence model is key to accurately predict the flow field distribution in the human respiratory tract, therefore, their analyzes were performed on four turbulence models, (LRN $\kappa-\epsilon$ model, RNG $\kappa-\epsilon$ model, SST $\kappa-\epsilon$ model and SST-Transition model). The SST-Transition model was found to be the best choice for predicting inhalation velocity profiles, whereas the RNG $\kappa-\epsilon$ model and SST $\kappa-\epsilon$ model were recommended to simulate the flow field in the respiratory tract during exhalation. On the turbulence note, Luo, Hinton, Liew, and Tan (2004) affirmed that flow in the HUA during *heavy-breathing* can have a Reynolds number as high as 9300, and therefore presents turbulent features, they studied transitional/turbulent flow using a *large eddy simulation* (LES) in a 2D and 3D asymmetric bifurcation models of human upper airway and the results demonstrated that the LES model is capable of capturing instantaneous eddy formation and flow separation in (almost) laminar, transitional and turbulent flow regimes, and hence, as they propose, it may be used as a powerful and practical tool to provide much of the detailed flow information required for tracing the *particle trajectories* and *particle deposition* in human airways. Later, on a similar study performed by Mylavarapu et al. (2009), an anatomically accurate HUA model was constructed from multiple magnetic resonance imaging axial scans, as well as an identical physical model of the same airway using stereo lithography. Pressure and velocity measurements were conducted and five different turbulence models considered to simulate at a peak expiratory flow rate of 200 L/min. They found that among all the approaches considered, the standard $\kappa - \omega$ turbulence model resulted in the best agreement with the static pressure measurements. Finally, V. K. Srivastav, Paul, and Jain (2019) focused attention on capturing the wall turbulence by studying the local Reynold's Number in terms of the y^+ value for the near wall mesh refinement. They found vital the judicious selection of y^+ value and the turbulence models to correctly simulate airflow in respiratory tract at heavy-breathing conditions.

As to the spatial discretization assumption, Cui, Wu, and Gutheil (2018) investigated the characteristics of both steady and unsteady airflow structures in an idealized mouth-throat using LES; that study provided evidence about the physical processes leading to both enlarged mixing zones and recirculation zones, as well as evidence on the fact that both airflow structures show distinct properties at light and heavy breathing conditions, particularly in the unsteady flow field. Another study considering steady and cyclic unsteady conditions in oral and nasal breathing routes is that of Paz, SuÁrez, Concheiro, and Porteiro (2017), were the airflow distributions through oral and nasal routes were determined, analyzed and compared under different breathing conditions, and significant differences in turbulent intensity contours between steady and unsteady cases were observed.

Regarding the flow pattern, most studies (X. Xu et al., 2020) agree upon the fact that the flow distribution in the trachea under exhalation is quite different from that under inhalation condition; moreover, due to the inclination of the trachea region, the unique shape of the respiratory tract and the constricted cross-sectional area of the throat and glottis, the airflow passing the glottis is accelerated. This phenomena is found on the literature as *glottal jet*. Shang, Dong, Tian, Inthavong, and Tu (2020) obtains on a similar study regional airflow in terms of axial velocity and secondary flow vorticity along the lung airway model, paying special attention on the lower lung airways. Furthermore, obvious secondary flow currents were captured in the larynx-trachea segment and left main bronchus, while for the terminal conducting airway in the right lower lobe, the airflow tends to be much smoother with no secondary flow currents. Calay, Kurujareon, and Holdø (2002) studied the respiratory flow patterns for normal breathing and maximal exercise conditions on 3D asymmetric bifurcation model of the central airway. They found that flow patterns on those cases are strongly dependent on the convective effect and the viscous effect with some contribution of the unsteadiness effect; besides, found the difference between the two cases to be the flow separation regions:

close to the carinal ridge for maximal exercise condition, and no separation regions observed for the normal breathing one. Additionally, Karaman and Tsega (2018) used CFD to study the age-related effects on inspiratory and expiratory airflow dynamics in four-generation lung airway models under normal breathing conditions. The obtained results indicate that as age increases, airflow velocity, pressure, and wall shear stress decrease for both inspiration and expiration in a particular sub-region of the respiratory tract. Furthermore, during inspiration, the splitting of velocity streamlines at bifurcations was found to increase with age.

To summarizing, when it comes to analyzing the flow patterns and fluid dynamics on the HUA there are three major factors to account for, the volume rate, which could be of inspiration or expiration with different intensities; the geometry, and how accurately describes the real HUA, and turbulence models. Velocity profiles and pressure measurements here obtained are of relevance to better understand the fluid's behavior and contribute to medicine, especially when researching obstructed airways and surgery planning. This study type also establishes the precedent for correctly analyzing other phenomena such as particle deposition and air-wall stresses, as we shall see later on.

2.2 PARTICLE TRAJECTORY AND DEPOSITION

Several numerical studies have been conducted on this topic to the date, since, as pointed out by Zhang and Kleinstreuer (2011), deposition in the human lung is of great environmental and biomedical concern, especially for children, asthmatics and the elderly; One area of high level research activity is that of atomization and sprays which are also applicable for the drug delivery devices (Ahmadi, 2013). Modeling the motion of particle suspensions in a viscous fluid is a wide research area, which goes far beyond the scope of this brief state of the art, the aim of this section is simply mention some relevant studies performed on this area, and that have contribute to the author on the construction of the mathematical set of equations for the simulations to be performed on the framework of the present thesis.

When it comes to text books on this topic, Maury (2013) presents an interesting basic explanation on how computed velocity field can be used to follow the motion (and possibly the deposition) of particles in the respiratory tract; including sections such as *particle in a moving fluid* and *particle in a bifurcation*, besides illustrative exercises. There is also the work of Ahmadi (2013), where the *Computational Fluid and Particle Dynamics* (CFPD) is proposed as an extension of the CFD knowledge with additional modelling requirements to reflect the particle dynamics within the fluid flow. They point out one major advantage of CFPD as the ability to simulate fluid-particle flows that are not reproducible in any experimental tests. This is especially significant in the medical and pharmaceutical fields where invasive experimental setups that deal with human subjects are difficult to undertake, as it is the case of mechanically ventilated patients. The book also contains a comprehensive review of relevant applications of CFPD approaches, for example: pulmonary drug delivery, nasal drug delivery, therapies for sleep apnea, studies in the acinus and olfactory regions, and assistance to nasal surgery. Finally, from the mathematical point of view their contribution is imperative to all whom wish to study the particle transport, dispersion and deposition phenomena. The sixth chapter focuses on the fundamentals of particle dynamics considering the Eulerian and Lagrangian approaches, in order to understand how particles move through the respiratory airway; they explain the basic terminology to understand the context, and to distinguish it from other fields that study particles (i.e. quantum, nuclear physics).

One very complete and relevant study, made within the framework of a doctoral degree is that of Cui (2012) which studied the airflow field and particle dispersion and deposition in the human upper respiratory system on four different geometries; besides treating the turbulence effect by means of LES model. They considered one-way and two-way coupling depending upon the different particle volume fraction and Lagrangian equations were used to describe particle motion. Particle deposition efficiency, particle deposition pattern on the surface, the relationship between the final particle positions and released particle positions at the inlet palate, and the particle trajectories were studied. They found that all were greatly dependent on the particle size, inspiration flow rate and initial particle position. The turbulence and recirculated flow were found to have great influence on the particle trajectories. Particles with 2 μm could pass through the pharynx. However, they could not go into the deep site totally due to the filtering function of trachea; the large particles could not even pass through the pharynx. Furthermore, it is also important to mention the work of Vaish (2014) as a thesis submitted for the degree of Master of Science, where he explored and validated OpenFOAM software to simulate lung-aerosol dynamics in realistic human airway models, making comparisons between simulation results with OpenFOAM and the commercial solver CFX (Ansys, Inc. Canonsburg, PA) for one steady and one transient case, focusing on clock time and accuracy, concluding that simulated particle trajectories using OpenFOAM's Lagrangian Particle Tracking solver *icoUncoupledKinematicParcelFoam* constitutes a valid approach. He also compared particle deposition simulations results with in-vivo experimental studies.

There have also been related work published as scientific articles; we already mentioned that of Zhang and Kleinstreuer (2011) who considered the change of breathing routes had on deposition fractions and global surface concentrations on spherical nano-particles in the 1 to

100 μm mean diameter range employing an experimentally validated computer simulation model. They concluded that effect depended greatly on the particle size. The impact of different outlet flow-rate ratios generated by downstream resistances, e.g., caused by airway inflammation or tumors, was discussed in this study as well. It was found that different outlet pressures primarily influence the velocity profiles and nano-particle deposition fractions at that particular branch and adjacent bifurcations. Latter, on a connected work, Huang and Zhang (2011) analyzed transient airflow patterns and particle deposition during both inspiratory and expiratory processes in a realistic human upper respiratory tract model with 14 cartilaginous rings (CRs) in the tracheal tube, where the transient deposition fraction was found to be strongly depend on breathing flow rate and particle diameter but slightly on turbulence intensity. Besides, the deposition fraction in the trachea during expiration was found to be much higher than that during inspiration because of the stronger secondary flow.

V. Srivastav, Paul, and Jain (2012) extended the three dimensional respiratory tract from third to six generation bronchus based on Weibel model (which is an idealized symmetrical lung model based on regular pipes proposed in 1963). They performed laminar flow simulations taking into account aerosol-particles of 10 μm uniform diameters, and two phase flow by means of the Discrete phase modeling (DPM) feature in Ansys-Fluent-14. It was found that most of the particle deposits at the bifurcation junction because of the inertial impaction at this location. Thus, bifurcation junction is an important location from medical point of view. The DPM feature of Ansys-Fluent was also used on the work of Rahimi-Gorji, Pourmehran, Gorji-Bandpy, and Gorji (2015), where the airflow behavior and particle transport and deposition was investigated in three different breathing conditions. They found out that when changing the breathing conditions from light to intense, the major particle deposition zones changed on the realistic geometry they simulated. Also, the maximum pressure distribution happens when they simulated the maximum flow rate, and according to the results, the particles always tended to go to the right branch of the model. Moving on to open source software, Vaish, Kleinstreuer, Kolanjiyil, Saini, and Pillalamarri (2016) used OpenFOAM to simulate airflow and micro-sphere transport in a patient-specific lung airway model. They considered turbulent behavior as the laryngeal jet occurring in the throat region may induce turbulence immediately downstream, thus they validated a transitional turbulence model, and a modified eddy interaction model with a generalized near-wall correction factor. Particle depositions in the realistic lung-airway configuration were compared with those in an idealized upper airway model. Their results indicated that for micro-sphere deposition in turbulent airflow regions, selecting an appropriate near-wall correction factor can reduce the problem of subject variability for different lung-airway configurations.

Cui and Gutheil (2017) compared effects of steady and unsteady flow fields when simulating an idealized human mouth throat under the different inspiration flow rates. They used the LES model and Lagrangian particle tracking to investigate the process of particle drug delivery for medical treatment of the human airway. They found that the mono-disperse particles may follow totally different trajectories depending on their initial release positions and the inspiration flow rates as well as on their size. The particles may follow very complex recirculating movements within the recirculation zone, and they may show a swinging, transverse or helical motion due to the vortex of the gas flow, which in general, may affect the deposition characteristics of the injected particles. A very similar study is that of Ghahramani, Abouali, Emdad, and Ahmadi (2017), they also used LES technique and the Lagrangian approach to calculate the trajectories and deposition of micro particles for two different breathing rates. They compared the results with previous ones using the RANS model and it was found that the results obtained by the LES method for the total depositions of microparticles are comparable with those of the RANS model. The regional particle deposition, however, showed marked differences. In addition, significant differences were found in the predicted airflow characteristics. That same year an interesting work was submitted by X. Y. Xu et al. (2017), were a realistic three dimensional human upper airway model including the nasal, oral, pharynx, larynx, trachea and part of the first generation of the tracheobronchial tree, as well as a tissue region from the pharynx to the upper bronchi. The *Transition Shear Stress Transport* (SST Transition) turbulence model, Penne's bio heat transfer equation, convective boundary conditions and a Lagrangian frame were applied and verified with experimental measurements to simulate the airflow fields, temperature distributions and particle deposition in the model. The effects of flow rate, inhalation temperature and particle diameter were studied since their motivation lies on the fact that inhalation injury from exposure to fire smoke is one of the causes of burn related death.

Recent studies are those by Deng et al. (2019) and Kim, Tong, Chan, and Yang (2019). They first investigated health effects resulting from physical activity in polluted air by looking at particle deposition in human tracheobronchial (TB) airways using a CFD method. They found that particle deposition is strongly affected by physical activity; the difference in the deposition pattern was due to the reason that physical activity increased the airflow which increased inertial impaction. The study showed that there are different health effects for different activity levels: sedentary activity leads to chronic health effects, intense activity results in acute effects, and moderate activity minimizes the adverse health effects of physical activity in polluted air.The second mentioned paper presented a CFD study of air and particle flows in a realistic parametrically controlled airway model developed by Kitaoka under different inspiratory conditions. The results were analyzed with simulation data obtained in the classic Weibel airway (WA) model and compared with previous experimental and simulation studies. The study demonstrated that the Kitaoka model has a great potential in modeling lung deposition of particles under different conditions. It is important to mention that the experimental methods for flow and aerosol measurements in human airways have also been reviewed. Two important papers on this regard are that by Lizal et al. (2018) and the one of Chan and Lippmann (1980).

Finally, as mentioned before, important parameters in this research field include particle size, initial position, and flow rates. Most studies focus on drug delivery or contaminant agent deposition, both relevant topics in modern days; however, there is no much research, to the author's knowledge, simulating physiological phenomena involving organic particles (saliva, gastric reflux, among others) through the respiratory or digestive tract, this is considered to be a phenomenon to study on the present work.

2.3 FLUID STRUCTURE INTERACTION

Up to this point, the literature suggests that most studies conducted on this field are related to HUA simulation and considerably focuses on the aspects of fluid dynamics or particle deposition, as briefly reviewed on the previous sections. However, there seems to be a gap in obtaining information on the effects of *fluid-structure interaction* (FSI). The application of FSI in HUA is still limited in the literature; as such, this next section attempts to discuss the models used so far to modeling the stresses and strains on the HUA air wall when submitted to different flow conditions.

The computation of FSI problems requires the solution of the coupled fluid and solid underlying governing equations (Wall & Rabczuk, 2008), and as the two sub problems, which are the incompressible Navier-Stokes equations for the fluid, and an elastic solid equation for the solid, are big mathematical challenges on their own, it is no surprise that results for the coupled problem are rarely spread.(Richter, 2017)

In the present research we are interested in knowing the principal stresses and strains under which the trachea is submitted when the patient is under mechanical ventilation, because, as stated by Malvè, del Palomar, López-Villalobos, Ginel, and Doblaré (2010), the trachea as a construction is a reinforced tube. Sixteen to twenty cartilaginous half-rings whose ends are connected by a soft membranous wall form the anterior tracheal wall, and understanding the breathing process of forced ventilation in a trachea model, and how the airflow and stresses in the airway wall are distributed are essential in order to design more convenient prostheses or mechanical ventilation techniques, as it is the aim of this project for the design of the endotracheal cuff.

On this area some important contributions to the scientific community have been made. Some of the most relevant references to the author on the basics of FSI can be found on Richter (2017), as well as basics of the approach with implementations to the *finite element method* (FEM), on Bathe, Hou Zhang, and Ji (1999); Bathe and Zhang (2004). The work of Bhalla, Bale, Griffith, and Patankar (2013) where an *immerse boundary method* (IB) is used as a mathematical framework to simulate rigid, deforming, and elastic bodies. Furthermore, some mixed approaches can also be found, such as the *boundary element method* (BEM) and FEM, for example that of Park, Koh, and Kim (1992), and combinations of conventional CFD-DEM models.

On the biomedical field of research most documented FSI computations have been on the cardiovascular branch (Necasová, 2014). However, Wall and Rabczuk (2008) studied the deformability of airway walls, airflow patterns and airway wall stresses in the first generations of lower airways in a real lung geometry trough a partitioned FSI approach solving transient incompressible Newtonian flows and (geometrically) non-linear airway wall behavior. They studied models for healthy and diseased lungs, and both normal breathing and mechanical ventilation scenarios are studied. It was concluded that airflow patterns, both axial and in-plane, were quite different between CFD and FSI simulations, especially in lower generations. Furthermore, the maximum stresses found were below $300kPa$.

Malvè et al. (2010) used a FEM model of a human trachea to analyze the deformability of the tracheal walls under coughing. Tracheal wall was modeled as an anisotropic fiber reinforced hyper elastic solid material in which the different orientation of the fibers was accounted for. The implantation of an endotracheal prosthesis was simulated, which is of great importance for the present research, since, that research can be considered as a first approach to analyze the influence of a tracheal stent implantation in a patient, since it is capable of giving information on the muscular wall deformation, and flow patterns coming out the trachea. To demonstrate a possible clinical application of this numerical model, they simulated the same human trachea in presence of a endotracheal prosthesis, modeled as a simplified 2D cylinder. In the region where the tracheal stent was placed, the muscular membrane could not collapse because the material stiffness prevents the wall prostheses from it. Then, the differences in the flow regime between the healthy trachea (with flexible membrane) and the trachea with the silicone stent were analyzed. the calculated velocity field of the air flowing out the trachea in presence of stent showed lower velocity gradients in comparison with a cough in a healthy trachea. Next, Malvè et al. (2011) focused on the analysis of the response of the tracheal wall to different ventilation conditions. Normal breathing was performed assuming a sinus shape of the pressure at the inlet and air speed at the outlet, based on real data which represent the inspiration and the expiration processes respectively. Mechanical ventilation was simulated considering positive values of pressure using data from a mechanical ventilation machine. Deformations of the tracheal cartilage rings and of the muscle membrane, as well as the maximum principal stresses in the wall, were analyzed. The results showed that, although the deformation and stresses are quite small for both conditions, forced ventilation does not exactly imitate the physiological response of the trachea, since with always positive pressure values the trachea does not collapse during mechanical breathing. However, one interesting finding is that the level of stresses for the mechanical ventilation was found to be more than twice higher than for normal breathing. Higher stresses are related with higher risk, and in this sense, the behavior of the trachea under both conditions is not the same.

Finally, Dailey and Ghadiali (2007) developed a 2D fluid-structure computational model of alveolar dynamics to quantify how these parameters influence particle transport in the deep lung. Meaning that on a single study brought together the particle transport and FSI phenomena in deformable pulmonary alveoli. Results indicate that Brownian diffusion dominates the transport of small particles, while gravitational sedimentation dominates the transport of large particles. Mid-size particles experienced slower diffusion and slower sedimentation transport, so their time to impaction is maximized. Furthermore, stiffer tissues produced higher particle impaction rates under microgravity conditions while tissue viscosity had negligible effects on particle dynamics.

Closing this brief state of the art it is important to notice the fact that there are very few, virtually none research studying the mechanical ventilation condition and the endotracheal device design, including the cuff effectiveness, at least not with realistic geometries or turbulence conditions. This is the aim of the present research.

Part II

Numerical Simulations

Chapter 3

Computational Fluid Dynamics

CFD is a ramification derived from fluid mechanics theory that takes advantage of the technological advance in computing to bridge the gap between theoretical and experimental fluid dynamics. This is to be accomplished by solving fluid-flow related problems with iterative computerized computations when replacing the Navier-Stokes equations with a mathematical model. Such a model is based on discretized algebraic expressions that are integrated over each control volume defined for the problem according to the finite volume approach.

Given that the aim of this research is to perform simulation scenarios from a hierarchical approach (using each time increasingly more complex mathematical models to describe the physics of the problem step by step), this first approximation attempts to replicate the study performed by (Luo et al., 2004) using the open source code OpenFOAM. Here we attempt to obtain detailed information about the flow field pattern, the fluid dynamics and turbulence influence on respiratory dynamics in a single asymmetric bifurcation model of human upper airway.

The layout of this paper is as follows. Detailed CFD theory is introduced in Section 3.1; this includes the governing equations for present phenomena and the *finite volume method* (FVM) implementation on OpenFOAM. Modelling set up is found on Section **??**; here assumptions, model geometry, turbulence modelling and boundary conditions are discussed. Results of the flow patterns and path lines using LES, $\kappa - \epsilon$, and laminar models are presented in Section 3. Discussions and conclusions are given in Sections 4 and 5.

3.1 MATHEMATICAL MODEL

3.1.1 GOVERNING EQUATIONS

The governing equations of fluid flow represent mathematical statements of the conservation laws of physics (Versteeg & Malalasekera, 1995), the purpose of this section is to provide a glimpse of the theoretical background behind the concepts of the fluid dynamic from the basic principles of conservation of mass, momentum, and energy.

In analyzing phenomena regarding fluid flow it is assumed that the fluid is a *continuum*, meaning that its properties are defined at every point in space; within that assumption, fluid flow behavior can be categorized as either Newtonian or non-Newtonian. For the problem proposed on this investigation, the author is concerned only in the physics and behavior of Newtonian fluids, which are distinguished by the linear relationship between their shear stress and their shear rate, with their molecular viscosity μ, (which is a measure of the ability of a fluid subjected to stress to resist deformation) (Moukalled, Mangani, & Darwish, 2015). Flows can also be classified mathematically according to the partial differential equations describing them. As will be shown in the following sections, fluid flows are governed by the Navier-Stokes equations, which are nonlinear second-order partial differential equations in four independent variables. In general, flows are unsteady and three dimensional.

3.1.2 REYNOLDS-AVERAGED NAVIER-STOKES EQUATIONS FOR A NEWTONIAN FLUID

The system of equations that governs the time-dependent three dimensional fluid flow for an incompressible Newtonian fluid are represented as follow,

$$\frac{\partial \rho}{\partial t} + div(\mathbf{u}) = 0 \tag{3.1}$$

$$\rho \left[\frac{\partial u}{\partial t} + div(u\mathbf{u}) \right] = -\frac{\partial p}{\partial x} + div(\mu grad u) + S_{M_x} \tag{3.2}$$

$$\rho \left[\frac{\partial v}{\partial t} + div(v\mathbf{u}) \right] = -\frac{\partial p}{\partial y} + div(\mu grad v) + S_{M_y} \tag{3.3}$$

$$\rho \left[\frac{\partial w}{\partial t} + div(w\mathbf{u}) \right] = -\frac{\partial p}{\partial z} + div(\mu grad w) + S_{M_z} \tag{3.4}$$

Where Equation 3.1 accounts for a mass balance in which the rate of increase of mass in the fluid element equals the net rate of flow of mass into the fluid element. Equations 3.2 to 3.4 follow the statement that the rate of change of momentum of a fluid particle equals the sum of the forces on the particle. In addition, $\mathbf{u}$ stands for the velocity vector, where (u, v, w) are its respective components, p is the pressure, μ is the dynamic viscosity, ρ the density and S_{M_x} accounts for the moment source term.

3.1.3 FINITE VOLUME METHOD

If one decides to introduce to these equations a general variable named ϕ, it can be obtained the general transport equation (3.5), which is used as a starting point for computational procedures in the FVM, as indicated by Versteeg and Malalasekera (1995). This equation has transient, convection, diffusion and source terms, where each term brings a characteristic contribution to the equation that needs to be reproduced by the discretization procedure (Moukalled et al., 2015).

The key step of the method relies on the integration of the Equation 3.5 over a three-dimensional control volume CV to yield a discretized equation at its nodal point P, (Equation 3.6). The method began with the one-dimensional steady-state diffusion equation, which is the simplest transport process of all, and then it was extended to two and three-dimensional convection-diffusion problems.

$$\rho \left[\frac{\partial \phi}{\partial t} + div(\phi\mathbf{u}) \right] = div(\Gamma grad\phi) + S_{\phi} \tag{3.5}$$

$$\rho \left[\int_{V_P} \frac{\partial \phi}{\partial t} dV + \int_{V_P} div(\phi\mathbf{u}) dV - \int_{V_P} div(\Gamma grad\phi) dV \right] = \int_{V_P} S_{\phi} dV \tag{3.6}$$

Once the domain is divided into a finite number of arbitrary cells, the solution is sought inside each control volume and the only requirement is that the elements needs to be convex and the faces that made up the control volume need to be planar. As one wants to solve the general transport equation for the transported quantity ϕ in the domain, with given boundary conditions BC and initial conditions IC, it is important to know which control volumes are internal and which control volumes lie on the boundaries. On that note, one important remark is that the FVM makes it truly simple to implement a variety of boundary conditions in a noninvasive manner since as mentioned before, the unknown variables are evaluated at the centroids of the volume elements, not at their boundary faces (Moukalled et al., 2015). That characteristic has made the Finite Volume Method quite suitable for the numerical simulation of a variety of applications involving fluid flow.

At this point in the methodology, it is assumed that the values of all variables are computed and stored in the centroid of the control volume and that they are represented by the mean value. The next step is to convert the volume integrals into surface ones by means of the Gauss theorem, and the problem then is reduced to interpolating the cell-centered values (known quantities) to the face centers. After integrating, the semi-discrete Equation 3.7 is obtained. Where $S_f \cdot (\rho \mathbf{u} \phi)$ is the convective flux and $S_f \cdot (\rho \Gamma_\phi div\phi)$ is the diffusive flux.

$$\int_{V_P} \frac{\partial \phi \rho}{\partial t} dV + \sum_f S_f \cdot (\rho \mathbf{u} \phi)_f - \sum_f S_f \cdot (\rho \Gamma_\phi div\phi)_f = S_c V_P + S_p V_P \phi_P \tag{3.7}$$

The face values appearing in the convective and diffusive fluxes have to be computed by some form of interpolation from the centroid values of the control volumes at both sides of face *f*. At this point, it is important to mention that the diffusion process affects the distribution of a transported quantity along its gradients in all directions, whereas convection spreads influences only in the flow direction. Here rises the principal problem in the discretization of the convective terms, which is: the calculation of the value of the transported quantity ϕ at the control volume faces and its convective flux across the boundaries (Versteeg & Malalasekera, 1995).

Now, the discretization of the solution domain implies the creation of the mesh on which the governing equations will be solved (Lorenzo, 2016). This requires the subdivision of the domain into discrete non-overlapping cells or elements that completely fill the computational domain, wherein all cases the mesh is composed of discrete elements defined by a set of vertices and bounded by faces (Versteeg & Malalasekera, 1995). Consider the cell shown in Figure 3.1.

According to the FVM, and in agreement with Guerrero (2019), one should know about each cell, the following information: The control volume V_P has a volume V and has a centroid, which is point $\mathbf{P}$. Considering a contiguous cell with control volume V_N, the vector from the centroid $\mathbf{P}$ of V_P to the centroid $\mathbf{N}$ of V_N is named $\boldsymbol{d}$; the method also requires that all neighbors V_N of the control volume V_P are known. The control volume faces are labeled *f*, which also denotes the face center; The location where the vector $\boldsymbol{d}$ intersects a face is f_i. The face area vector V_f is located at the face centroid, is normal to the face and has a magnitude

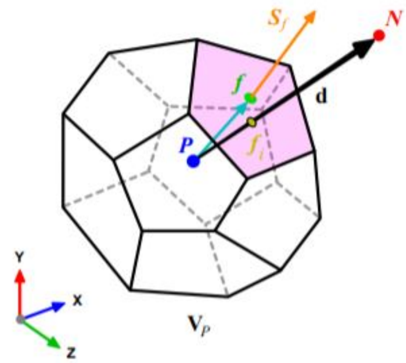

Figure 3.1. Cell on the solution domain. Taken from (Guerrero, 2019).

equal to the area of the face; finally, the blue vector from the centroid **P** to the face center f is named P_f.

As stated by Lorenzo (2016), a grid can be mainly of two types, according to where variables are located, collocated, and staggered. For a collocated grid, all the variables are defined at the computational point P. This can create issues when pressure and velocity are coupled. This problem can be solved by introducing a staggered grid, wherein the idea is to evaluate scalar variables at ordinary nodal points, but to calculate velocity components on staggered grids centered around the cell faces.

3.1.4 FVM DISCRETIZATION

The transport equation it's a non-linear second-order equation. First term is a temporal derivative, second is a convection term, then there is a diffusion term and finally the source term. For good accuracy, it is necessary for the order of the discretization to be equal to or higher than the order of the equation that is being discretized. (Guerrero, 2019)

- Convection term.

  The discretization of the convection term brings to Equation 3.8

$$\int_{V_P} div(\rho\phi\mathbf{u})dV \rightarrow \sum_f S_f \cdot (\rho\phi\mathbf{u})_f \tag{3.8}$$

  Where suffix f refers to the faces of the single control volume. Equation 3.8 needs the value of the parameter ϕ computed in the central point of the control volume, as well as the velocity and density values at each surface. That can be done through the *convection differencing scheme* that will be later explained.

- Diffusion term.

  The discretization of the diffusion term brings to Equation 3.9

$$\int_{V_P} div(\Gamma grad\phi)dV \rightarrow \sum_f S_f \cdot (\rho\Gamma_\phi div\phi)_f = S_c V_P \tag{3.9}$$

  In the case of having an orthogonal mesh, the diffusion term can be simply discretized by linearity. Non-orthogonality however, is usually more frequent and is the case for this study, wherein it is common practice to split this factor in two contributions, orthogonal and non- orthogonal, this is taken into consideration when choosing the numerical schemes.

- Source term.

  The discretization of the source term brings to Equation 3.10

$$\int_{V_P} S_\phi dV \rightarrow S_p V_P \phi_P \tag{3.10}$$

  Source terms can be addressed as function of ϕ. It can be as consequence linearized

Up to this point, the discretization scheme election becomes relevant, since one wants to use a finite number of cells and still have physically realistic numerical results. This could be achieved if the researcher has in mind the fundamental properties of discretization schemes: (i) conservativeness, (ii) boundedness and, (iii) transportiveness. The explanation of these properties, as well as the various discretization schemes to use, are beyond the scope of this article; however, with this brief introduction to what the FVM does, the reader would be able to further understand the choices made for the viscous-flow computations on the research.

3.2 NUMERICAL IMPLEMENTATION

3.2.1 THE GEOMETRIC MODELS

The idealized version of the airway is an smoother version of the one proposed by (Luo et al., 2004) but maintaining the key dimensions. In turn, they obtained it from another research where the dimensions were measured from the autopsy specimens of the human trachea and lungs, with no gross abnormalities. It is an asymmetric bifurcation model of only the trachea and the right and left bronchi.

The 3D model generated from the parameters in Table 3.1 is shown in Fig 3.2, (a).

	Diameter (mm)	Lenght (mm)	Angle (°)
Trachea	217	920	
Right bronchi	170	420	15
Left bronchi	126	530	30

Table 3.1. Dimensions used for the idealized model.

However, as it is the author's intention to compare not only differences in results between different turbulence models, but also geometry, a second, more realistic model is analyzed. This geometry was obtained by means of processing the CT scan images of an adult male patient.It is shown in Figure 3.2, (*b*).

The meshing process in OpenFOAM consist of initially define a domain which encloses the geometry for an hexahedral and uniform mesh, this is achieved by means of the *blockMesh* dictionary and command. Once this is achieved the *snappyHexMesh* utility generates 3D meshes containing hexahedra and split-hexahedra from a triangulated surface geometry in Stereolithography (STL) format. This is done on three steps: castellation, snapping, and boundary layer additiom, where all the volume and surface refinement is done in reference to the background (blockMesh) mesh.

Usually, the snappyHexMesh utility is used for external flow, however, it can also be used for internal flow, as it is the case for the present study. In order to indicate OpenFOAM that it is an internal flow mesh first, the user needs to define a closed STL geometry and a different STL file for each one of the boundary patches. For the geometrical models used here, there is one Inlet patch, two Outlets, (which are the right and left bifurcations), and the 'Volume' of Wall STL file. This files are readed and converted into .eMesh files by means of the *surfaceFeatureExtract* utility. Second, on the *snappyHexMesh* file the user needs to indicate a point defined by a variable named *locationInMesh* that needs to lie inside the geometry, in that manner, the utility understands that has to remove all cells outside that closed model, obtaining therefore the internal flow mesh.

The idealized model has 341214 cells of which the 90.25% correspond to hexahedra type, and the remaining has prisms and polyhedral. The realistic model has 998209 cells, of them 90.34% are hexahedra, besides a minor percentage of prisms, polyhedra and tet wedges. Both meshes were analyzed according to mesh quality parameters defined on *meshQualityDict* dictionary, and the *checkMesh* utility. All parameters have values within the normal or desired ranges.

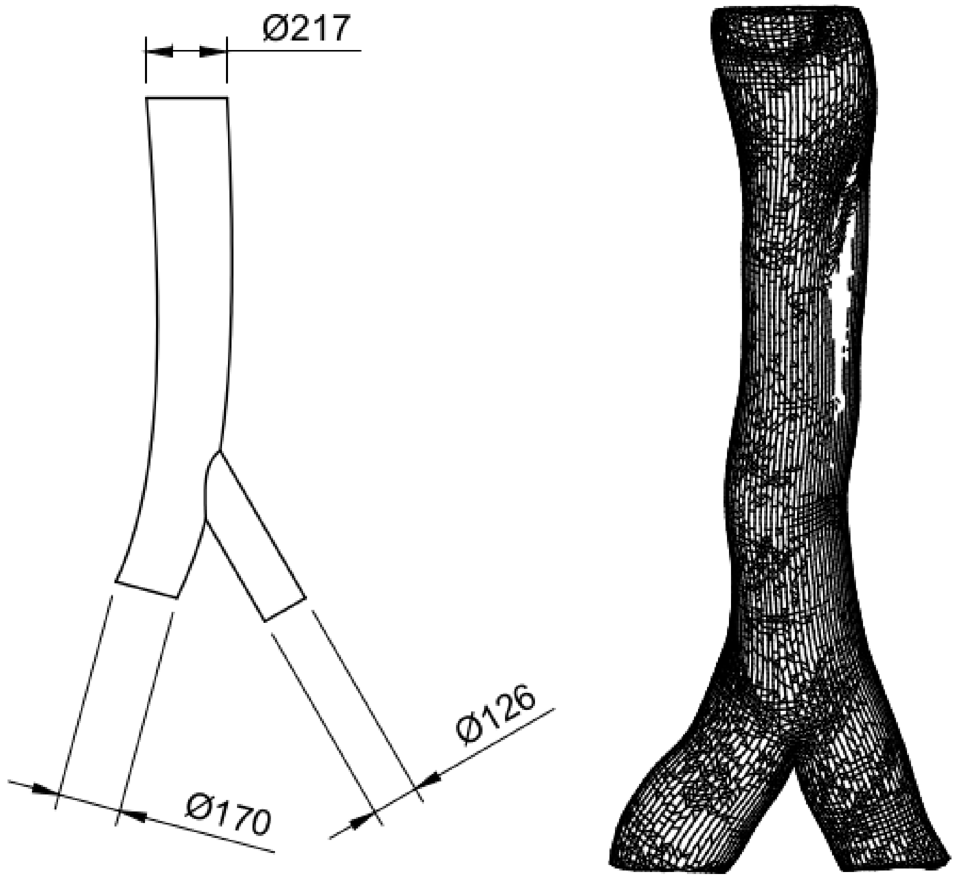

(a) (b)

Figure 3.2. Models used for viscous-flow simulations: (a) Idealized model. (b) Realistic model.

3.2.2 TURBULENCE MODELLING

Turbulence is a phenomenon of great complexity and the search for its mathematical understanding has challenged leading theoreticians for over a hundred years. The flow fluctuations associated with turbulence give rise to an additional transfer of momentum, heat, and mass (Versteeg & Malalasekera, 1995). Its appearance causes radical changes to the flow which can range from favorable (efficient mixing) to detrimental (high energy losses) depending on one's point of view.

Flow behavior can be described upon the *Reynolds number* (**Re**); this dimensionless quantity gives a measure of the relative importance of inertia forces (associated with convective effects) and viscous forces (Versteeg & Malalasekera, 1995). At low **Re**, the fluid's adjacent layers slide past each other smoothly and orderly; this is called the **laminar regime**. At high **Re**, the velocity and all other flow properties vary in a random and chaotic way; this regime is called **turbulent flow**. Flows in the laminar regime are completely described by the equations developed in Section 3.1.2. More complex flows can be tackled numerically with CFD techniques such as the FVM without additional approximations. The majority of engineering flows are turbulent, as it is the case for the flow to be studied for this research. It is known from the literature that the **Re**, in the trachea varies from 800 in light breathing (10 l/min) to about 9300 in heavy breathing (100 l/min) Luo et al. (2004), therefore, flow in the trachea is highly likely to be turbulent

Turbulent flows are characterized by eddies with a wide range of length and time scales.The *largest eddies* are typically comparable in size to the characteristic length of the mean flow, while the *smallest eddies* are responsible for the dissipation of turbulent kinetic energy Luo et al. (2004). What makes the prediction of the effects of turbulence so difficult is the wide range of length and time scales of motion, even in flows with very simple boundary conditions. Consequently, computational procedures need tools to cope with the complications that modeling turbulent behaviors have, this is to be done by mean of the **turbulence models**; A turbulence model is, as stated by Versteeg and Malalasekera (1995), a computational procedure to close the system of the equations that describe the flow's behavior. The classical models are based on the presumption that there exists an analogy between the action of viscous stresses and Reynolds stresses on the mean flow; the $\kappa - \epsilon$ model, for example, solves for the average velocity field. The *Large eddy simulations, LES*, on the other hand, are more sophisticated turbulence models where the time-dependent flow equations are solved for the mean flow, and the *largest eddies* and the effect of the *smaller eddies* are included to be modeled.

A mathematical discussion of the theory behind the aforementioned topics is beyond the scope of this introduction; however, it will be mentioned that, in agreement with Versteeg and Malalasekera (1995), the $\kappa - \epsilon$ is one of the most widely applied models and success in expressing the main features of many turbulent flows by means of one length scale and one time scale defining variable. The LES model, however has been found in other studies to be capable of capturing instantaneous eddy formation and flow separation in (almost) laminar, transitional and turbulent flow regimes, making it a useful and affordable tool for tracing the particle trajectories and particle deposition in human airways. That is why those two, besides the laminar model, will be considered for comparison on this first stage of numerical procedures. Details on $\kappa - \epsilon$ and LES mathematical modelling are given in Appendix A..

3.2.3 BOUNDARY CONDITIONS

The two types of boundary conditions that are most widely used are, the Dirichlet for general scalars, when a value is specified, and the Neumann boundary condition, when the flux is specified (Moukalled et al., 2015). Inside the *physical boundary conditions* the Dirichlet and Neumann conditions are applied, on this case, they may be referred as to *numerical boundary conditions.* On this study case, the numerical boundaries conditions used are:

- **Velocity**
  At the inlet and outlet is *freestream*, with a value of (2.0300), m/s. This boundary condition provides a 'mixed' condition derived from the inletOutlet condition, whereby the mode of operation switches between fixed (free stream) value and zero gradient based on the sign of the flux; meaning that if the flow is going outside, the boundary condition will be locally *zeroGradient*, if the flow is going inside, the boundary will be locally *fixedValue.* This is used in order to avoid results on which the flow returns to the computational domain.
- **Pressure**
  For pressure *freestreamPressure*, this pressure boundary condition uses a zero order extrapolation to compute the pressure at the boundary, meaning that is a *zeroGradient* condition but fixes the flux on the boundary to be (ρS_f*freestreamValue*).
- ϵ
  fixedValue of $\epsilon = 1.662452$ at the inlet and *zeroGradient* at the outlet.
- κ
  fixedValue of $\kappa = 0.062$ at the inlet and *zeroGradient* at the outlet.
- ν_t
  Calculated (uniform 0) for the $\kappa - \epsilon$ model. This boundary condition is not designed to be evaluated; it is assumed that the value is assigned via field assignment, on this case, the value of ν_t is calculated from the turbulence model and the values for κ and ϵ. The uniform (0 0 0) refers to a placeholder. For the LES model, the ν_t is also calculated, according to the Smagorinsky model, as explained in the Section **??**. The boundary conditions on that case is *zeroGradient.*
- **On the walls**
  no slip for velocity and *zeroGradient* for pressure, wall functions *nut-WallFunction* and *epsilonWallFunction*are used for the $\kappa - \epsilon$ model. No wall functions are used for the LES model.

The three dimensional domain is represented by $\Omega \subset \mathbf{R}^3$. And the domain boundary consist of $\partial\Omega = \partial\Omega_{wall} \cup \partial\Omega_{in} \cup \partial\Omega_{out1} \cup \partial\Omega_{out2}$, where them represent the wall, inlet and outlet boundaries, respectively. Here, the velocities on the boundary are defined as in Equation 3.11.

$$\mathbf{u}|\partial\Omega = \begin{cases} \mathbf{u}|\partial\Omega_{wall} & \text{is zero,} \\ \mathbf{u}|\partial\Omega_{in} & \text{is a constant value of given function,} \\ \mathbf{u}|\partial\Omega_{out} & \text{is computed by an outflow boundary condition.} \end{cases} \tag{3.11}$$

For the velocity, at the inlet the author considers inflow only on the y direction. Since for the laminar and RANS simulations the inflow is a steady flow, the constant flow rate at the inlet can lead to a *zeroGradient* at the outlet. Thus, the outflow boundary condition will reduce to a Dirichlet condition. For the walls, the *noSlip* condition is used. When it comes to pressure, all the boundary conditions are of Neumann type. the *freestreamPressure* used here is an outlet-inlet condition that uses the velocity orientation to continuously blend between zero gradient for normal inlet and fixed value for normal outlet flow. Then, the *zeroGradient* conditions are applied to the walls, the meaning is, the quantity is developed in space and its gradient is equal to zero in direction perpendicular to the patch (perpendicular to the walls). Figure 3.3 shows a schematic representation boundary conditions.

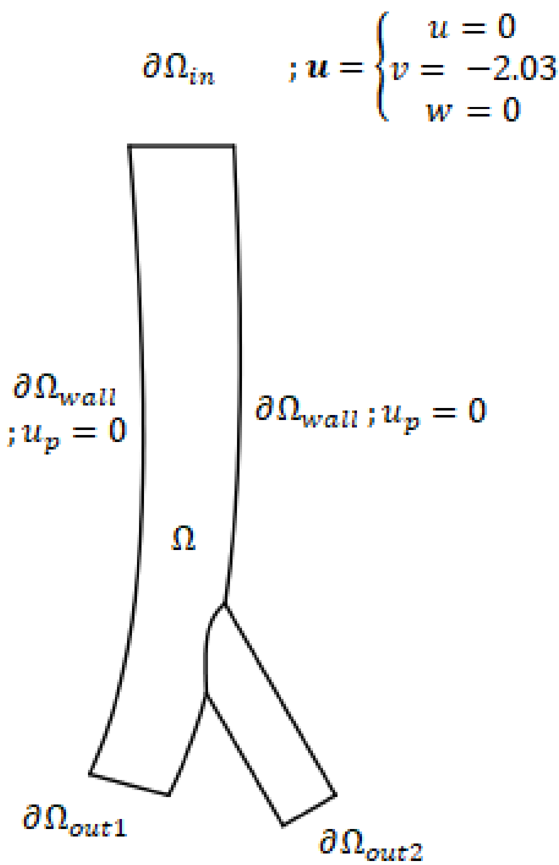

Figure 3.3. Schematic of boundary conditions used for initial viscous-flow simulations.

The information about physical boundaries is filed into the *constant* directory, inside the **polyMesh** folder. A summary of the parameters used for numerical simulation is given in Table 3.2.

Operating pressure	101 kPa
Physical properties	
Density, ρ Viscosity, μ	1.19 kg/m^3 1.82 x $10^{-5}kg/ms^{-1}$
Inspiratory rate	$45l/min$
Inlet velocity	$2.03m/s$
Re	3012

Table 3.2. Model's physical parameters.

3.2.4 NUMERICAL SCHEMES

The numerical schemes have been chosen, according to mesh quality, following instructions and suggestions provided by the OpenFOAM's documentation. The schemes for the laminar and RAS simulations are collected in the Table 3.3.

Numerical schemes	
ddtSchemes	default steadyState
gradSchemes	cellLimited Gauss linear 1
divSchemes	
default	bounded Gauss linearUpwind limited
turbulence	Gauss vanLeer
div((nuEffdev2(T(grad(U)))))	Gauss linear
laplacianSchemes	Gauss linear corrected
interpolationSchemes	linear
snGradSchemes	corrected
wallDist	method meshWave

Table 3.3. Numerical schemes Table for steady-state simulation.

Additionally, we have to change some of the parameters when simulating the under the LES model since on this case the time is also taken into account. On that case the numerical schemes are as in 3.4, and the time step used was $0.002s$ for the idealized geometry case-scenario, and $0.001s$ for the realistic geometry simulation. This was set in order to ensure a less-than-one Courant number (Co) for these transient simulations; a maximum of 1.18 Co was found for the idealized geometry, and maximum of 1.3 for the realistic geometry.

3.2.5 SOLVER EXECUTION

The general conservation equation dealt with in previous sections can be reformed into an equation similar to the continuity and momentum equations. Yet, in agreement with Moukalled et al. (2015), the numerical techniques presented up until now are not enough to allow for the resolution of the Navier-Stokes equations, and solving general fluid flows requires the use of algorithms that can deal with the coupling of pressure and velocity. This is of particular interest when dealing with incompressible flows, since the coupling between the aforementioned variables is very strong and because of the fact that pressure does not appear as a primary variable in either the momentum or continuity equations in this type of flow.

Numerical schemes	
ddtSchemes	default Euler
gradSchemes	cellLimited Gauss linear 1
divSchemes	
default	bounded Gauss linearUpwind limited
turbulence	Gauss vanLeer
div((nuEffdev2(T(grad(U)))))	Gauss linear
laplacianSchemes	Gauss linear corrected
interpolationSchemes	linear
snGradSchemes	corrected
wallDist	method meshWave

Table 3.4. Numerical schemes Table for transient simulation.

In OpenFOAM, the equation solvers, tolerances, and algorithms are controlled from the sub-dictionary **solvers** located in the *fvSolution* dictionary file, the **solvers** sub-dictionary specifies each linear-solver that is used for each equation being solved; The syntax for each entry uses a keyword that is the word relating to the variable being solved in the particular equation and the options related to the linear-solver.

On this research, the **GAMG** method (geometric-algebraic multi-grid), was chosen for symmetric matrices (e.g., pressure). The generalized method of (GAMG) generates first a quick solution on a mesh with a small number of cells; maps this solution onto a finer mesh, using it as an initial guess to obtain an accurate solution on the fine mesh. GAMG is faster than standard methods when the increase in speed by solving first on coarser meshes outweighs the additional costs of mesh refinement and mapping of field data (Guerrero, 2019). The agglomeration of cells is performed by the algorithm specified by the *agglomerator* keyword. On the present, the *faceAreaPair* method is used. Smoothing is specified by the *smoother*, since generally **GaussSeidel** is the most reliable option, is the one here proposed, an absolute tolerance equal to $1E-06$ and a relative tolerance **relTol** equal to 0.01 are used for this study.

For asymmetric matrices, the ones that are assembled from the velocity (U), and the transported quantities (κ, ϵ, T, and so on), was chosen the **smoothSolver** solver with smoother **symGaussSeidel**, an absolute tolerance equal to $1e-08$, since solving for these variables is relative inexpensive, so one can start right away with a tighter tolerance; and a relative tolerance equal to 0.1.

Note: The solver tolerance should represent the level at which the residual is small enough that the solution can be deemed sufficiently accurate. The solver relative tolerance limits the relative improvement from initial to final solution, since the linear solvers will iterate until reaching any of the tolerance values set by the author.

3.2.6 SOLUTION ALGORITHMS

The SIMPLE stands for Semi-Implicit Method for Pressure-Linked Equations, and is a pressure-corrector method. As stated by Moukalled et al. (2015). In the SIMPLE algorithm the solution is found iteratively by generating pressure and velocity fields that consecutively satisfy the momentum and continuity equations, while approaching the final solution (which satisfies both equations) at every iteration. This sequential, rather than simultaneous, solution of the equations is denoted in the literature by the segregated approach.

In OpenFOAM there is a sub-dictionary located in the dictionary file *fvSolution.* It controls the options related to the SIMPLE pressure-velocity coupling method. The SIMPLE method only makes 1 correction; however, an additional correction to account for mesh non-orthogonality is available, where he number of non-orthogonal correctors is specified by the *nNonOrthogonalCorrectors* keyword. The number of non-orthogonal correctors is chosen according to the mesh quality. For orthogonal meshes one can use 0, whereas, for non-orthogonal meshes it is recommended to do at least 1 correction, for the mesh obtained, the author chooses to use 3 corrections.

Additionally, OpenFOAM allows to also set the convergence controls based on residuals of fields. The controls are specified in the *residualControls* sub-dictionary of the dictionary file *fvSolution.* For this case-study the residual controls were set to $1e-5$.

A second sub-dictionary of fvSolution that is often used in OpenFOAM is relaxation factors which controls under-relaxation, a technique used for improving stability of a computation, particularly in solving steady-state problems. Under-relaxation works by limiting the amount which a variable changes from one iteration to the next, either by modifying the solution matrix and source prior to solving for a field or by modifying the field directly (Guerrero, 2019). An optimum choice for this values are the ones small enough to ensure stable computation but large enough to move the iterative process forward quickly; here a value of 0.3 is used for the pressure, κ and ϵ;and 0.7 for the velocity equation. The laminar and RAS simulations are conducted under this algorithm.

The PISO algorithm is used for the LES model. The letters stand for Pressure Implicit with Splitting of Operators. The splitting part comes when instead of solving all the coupled equations on an iterative fashion, it splits the operators into an implicit predictor and, multiple explicit corrector steps. Therefore it is not considered as an iterative scheme, which explains one of the main differences with the SIMPLE algorithm: not under-relaxation is applied and very few corrector steps are needed to obtain the desired accuracy. It is considered overall, an efficient method to solve the Navier-Stokes equations in unsteady problems.

3.3 RESULTS AND DISCUSSION

Taking advantage of the OpenFOAM functions, the author was able to obtain data from isosurfaces, streamlines, comparison of velocity magnitude and residuals information. On this section we attempt to analyze and compare quantitatively and qualitatively differences on results when varying turbulence models and geometry.

3.3.1 VELOCITY MAGNITUDE DISTRIBUTION

The magnitude of the velocity from the laminar, $\kappa - \epsilon$ and LES simulations are compared when evaluating three different profiles. There is one line crossing the models thorough the right bifurcation, one that crosses the left one, and a line “cutting”the trachea in order to evaluate the velocity profile. Let us compare also the results when the geometry varies.

It seems, from Figure 3.4 that there is a closest agreement between the results varying the turbulence models when the realistic geometry is analyzed. As for the idealized geometry, the turbulence models differ as the flow separates downstream from the trachea segment into the bifurcations, probably due to the LES ability to capture perturbations in the flow due to the pikes that this geometry has on these sections. This results can also be evidenced on Figure 3.5.

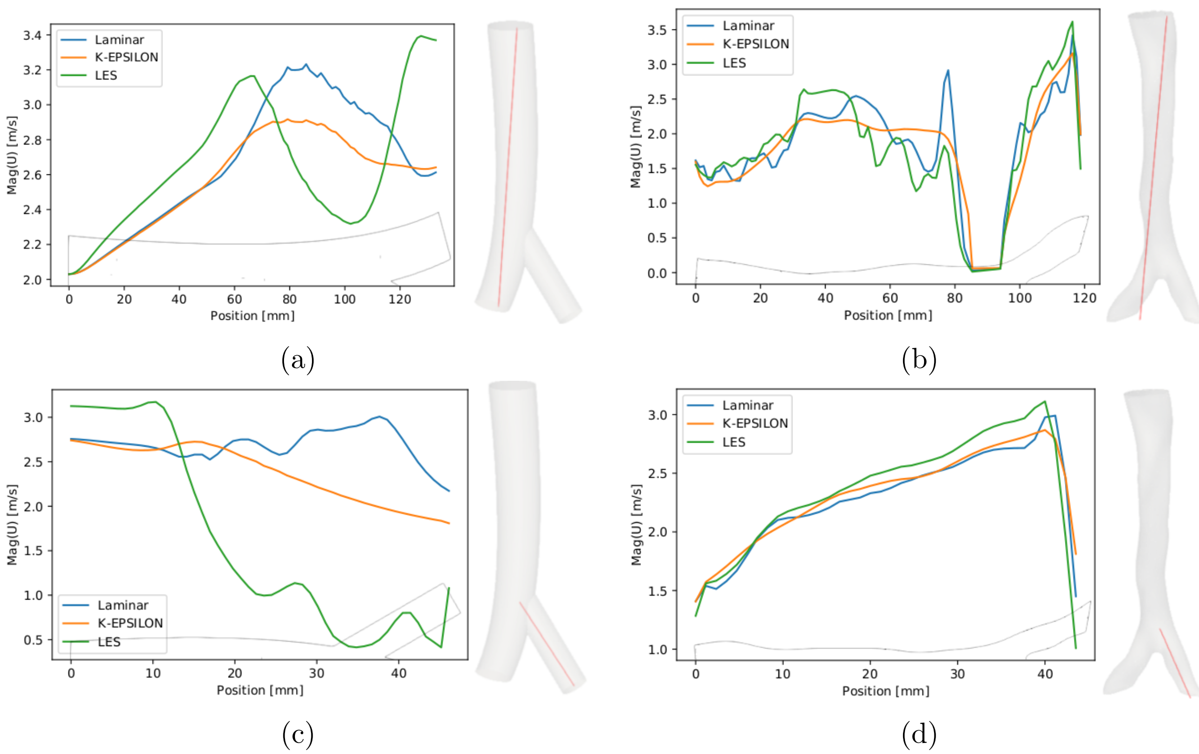

Figure 3.4. Comparison of the velocity magnitude distribution obtained using laminar, $\kappa - \epsilon$, and LES models: (a) Idealized model & (b) Realistic model along right bifurcation (c) Idealized model & (d) Realistic model along left bifurcation.

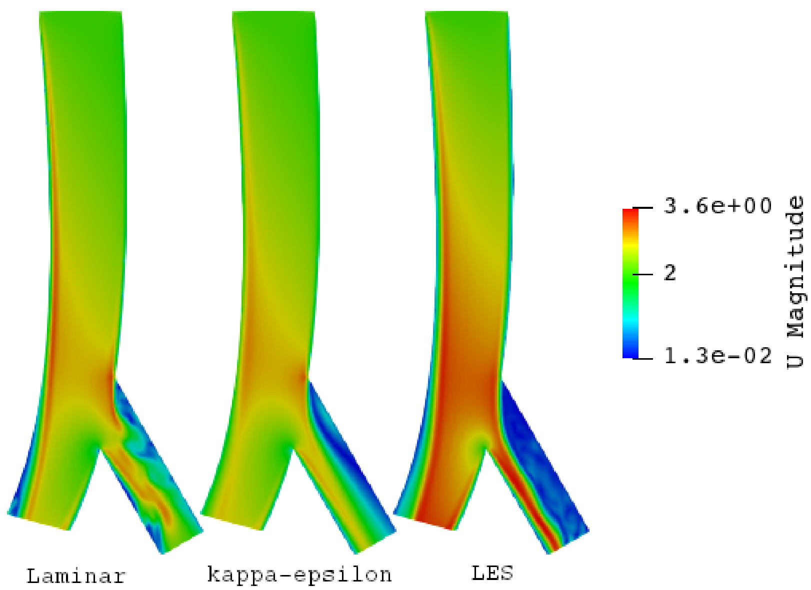

(a)

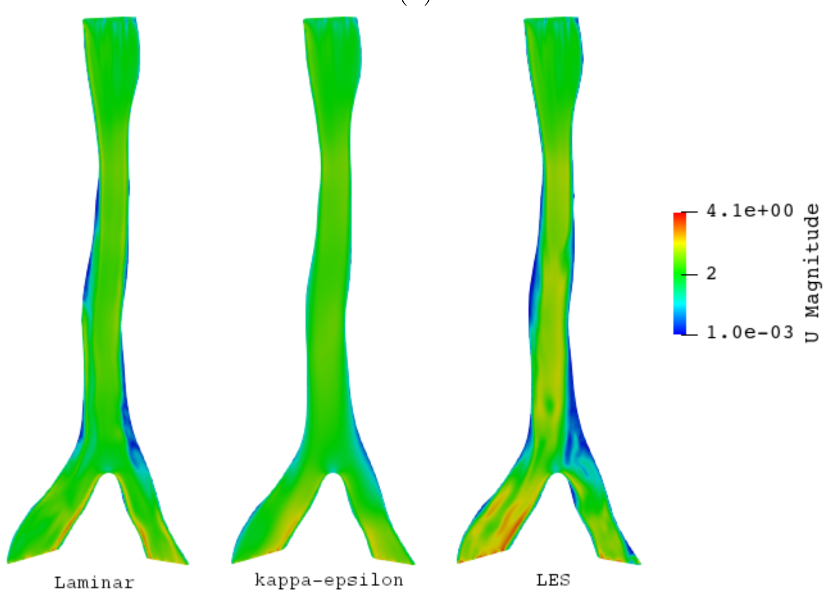

(b)

Figure 3.5. Velocity slices for the laminar, $\kappa - \epsilon$, and LES models, respectively for: (a) Idealized geometry, (b) Realistic geometry. .

Furthermore, the maximum velocities values found follow the same trend as in the article by (Luo et al., 2004) that is: the laminar maximum velocity is major than that registered for the $\kappa - \epsilon$ model, and the LES values are higher than the last two. Here we obtained $3.4m/s$, $3.2m/s$ and $3.6m/s$ respectively for the idealized geometry; and, $4.0m/s$, $3.8m/s$ and $4.1m/s$

for the realistic model. Additionally, the greater flow velocities occur in the right (bigger) bronchus, exhibiting a asymmetric velocity flow field between the two bronchi. At the tip of the bifurcation occurs a flow stagnation phenomena, obviously much more prominent on the idealized model due to that sharp edge. Besides, some flow separation is seen mainly on the left bronchi and with a hole lot of detail from the LES turbulence model, where the velocity profile develops showing also evidence of eddy formation.

The diameter-based velocity magnitude captured for both geometry models can be appreciated on Figure 3.6, where there is overall a good agreement between the turbulence models, of course, as seen before, the velocity values obtained with the LES model are higher than the others, and the laminar and LES models appear to have more in common compared with the $\kappa - \epsilon$ prediction.

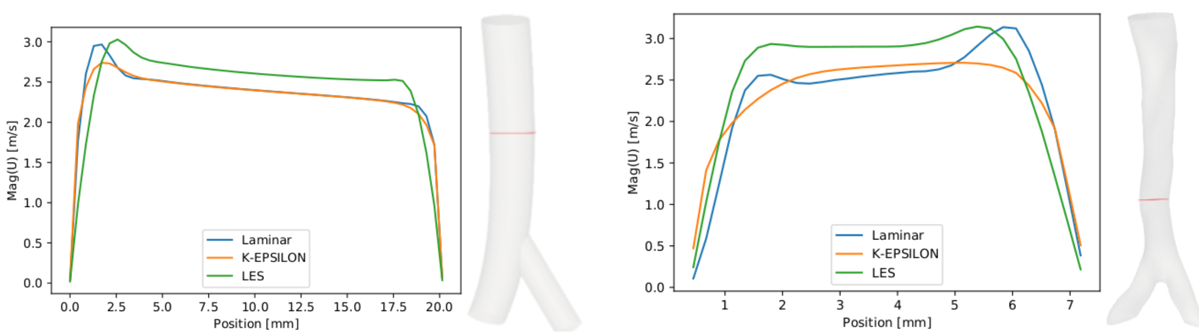

(a) (b)

Figure 3.6. Comparison of the velocity magnitude profile on the trachea obtained using laminar, $\kappa - \epsilon$, and LES models: (a) Idealized model. (b) Realistic model.

Typical instantaneous velocity contours for the idealized model are presented in Figure 3.7, where the maximum velocity is $3.6ms$ and we confirm that the velocity profile begins to change between predictions when and below approaching the bifurcation. There is also detailed evidence of the horseshoe profile also mentioned by Luo et al. (2004) on the LES results. Whereas the contours for the realistic geometry may suggest a much less turbulent behavior than its idealized counterpart. The maximum velocity on this case is $4.1ms$ and a more stable velocity profile is evidenced, which is in agreement with aforementioned graphs of velocity magnitude distribution along the right and left bronchi.

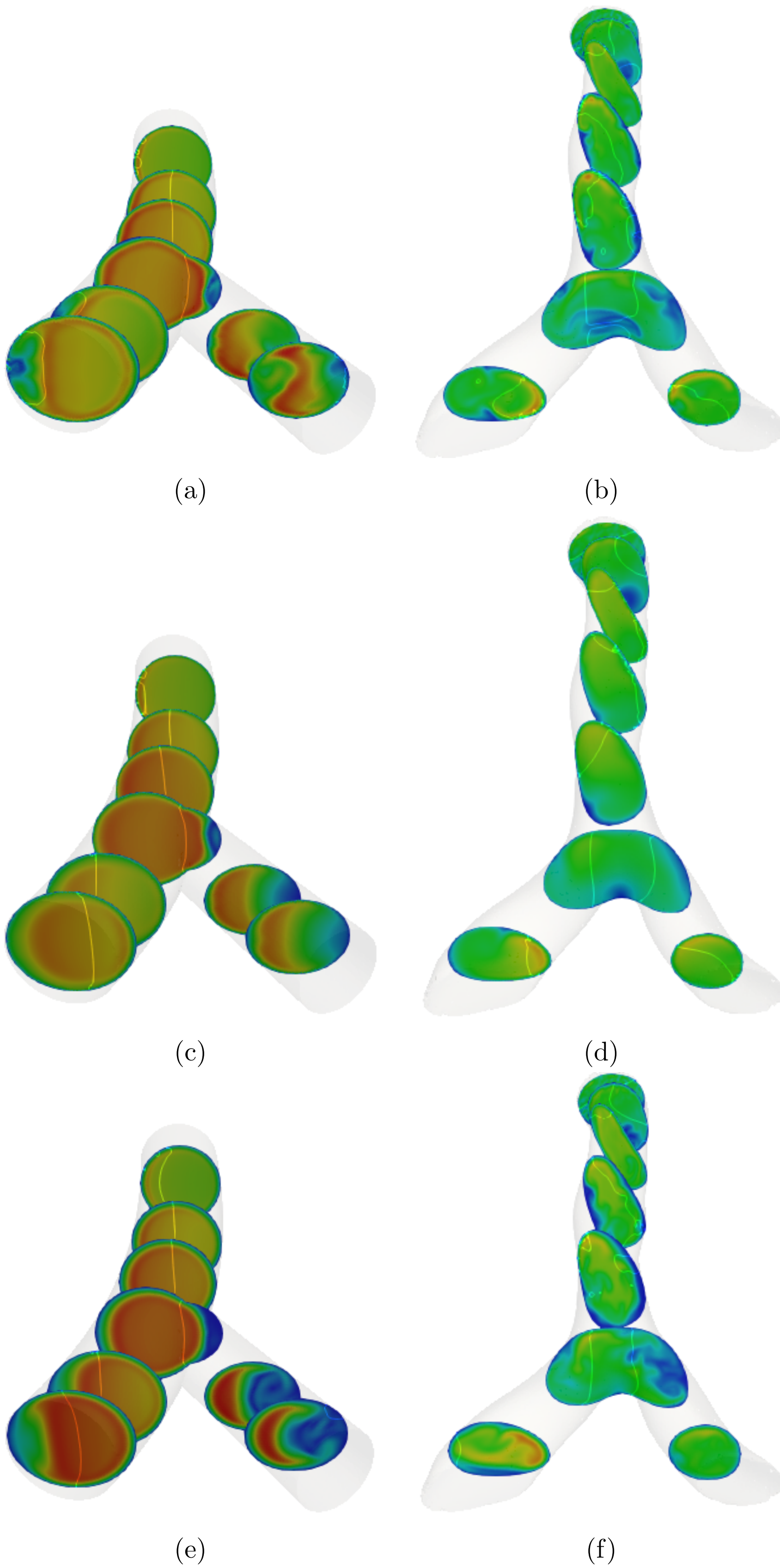

Figure 3.7. 3D instantaneous velocity contour at 6 intervals for both geometries. (a & b) Laminar,(c & d) $\kappa - \epsilon$, (e & f) LES.

3.3.2 STREAMLINES

While it is true we are interested on particle deposition for the cuff's seal evaluation, we have not yet, to this point, solve the particle coupling to the governing equations, therefore, for this "preliminar"type of study, we will have some look at the streamlines of the flow obtained from the actual simulations. Furthermore, while the steady-state simulations (laminar and $\kappa - \epsilon$ models) can also provide this type of graphical representation, these are only an approximation of what may happen to inhaled particles under the flow conditions here proposed.Comparison between streamline behavior can be found in Figure 3.8. Once again, the LES model shows a wavering pattern and flow separation in the left bronchus, whereas the $\kappa - \epsilon$ and laminar models appear to smear this behavior. It is clear from this depictions that very different flow patterns and therefore possible particles depositions would arose depending upon the geometric model chosen. A more detailed-realistic geometry combined with LES turbulence model are more likely to give a more accurate prediction of the particle deposition in the HUA.

3.3.3 RESIDUALS

As explained on Section 3.2.6, the residuals are set under the SIMPLE or PISO algorithms in order to account for convergence criteria and overall evaluation on the variables behavior. On this section we will see those residuals for velocity and pressure variables, along the entire simulation range, which was of 2000 iterations for all simulations.

The behavior of the initial residuals for the velocity and pressure variables are presented in Figure 3.9. These representations give good indication of what possible geometry-turbulence models configuration to use. When it comes to the idealized geometry the best behavior seems to be accomplished with the $\kappa - \epsilon$ model. Whereas for the realistic geometry the LES model excels in comparison with the other two. This is reaffirmed when looking at the respective histograms on Figure 3.10, where the aforementioned geometry-turbulence choices also exhibit the most normalized distribution among the rest. The mean value for the U_y velocity for the idealized geometry with $\kappa - \epsilon$ model is $5.043165e - 09$ with standard deviation of $1.754026e - 09$. The mean value for the realistic geometry with LES model is $3.174977e - 09$ with standard deviation of $2.617892e - 09$. All residuals go below the convergence parameter, which was set to the range of $1e - 5$.

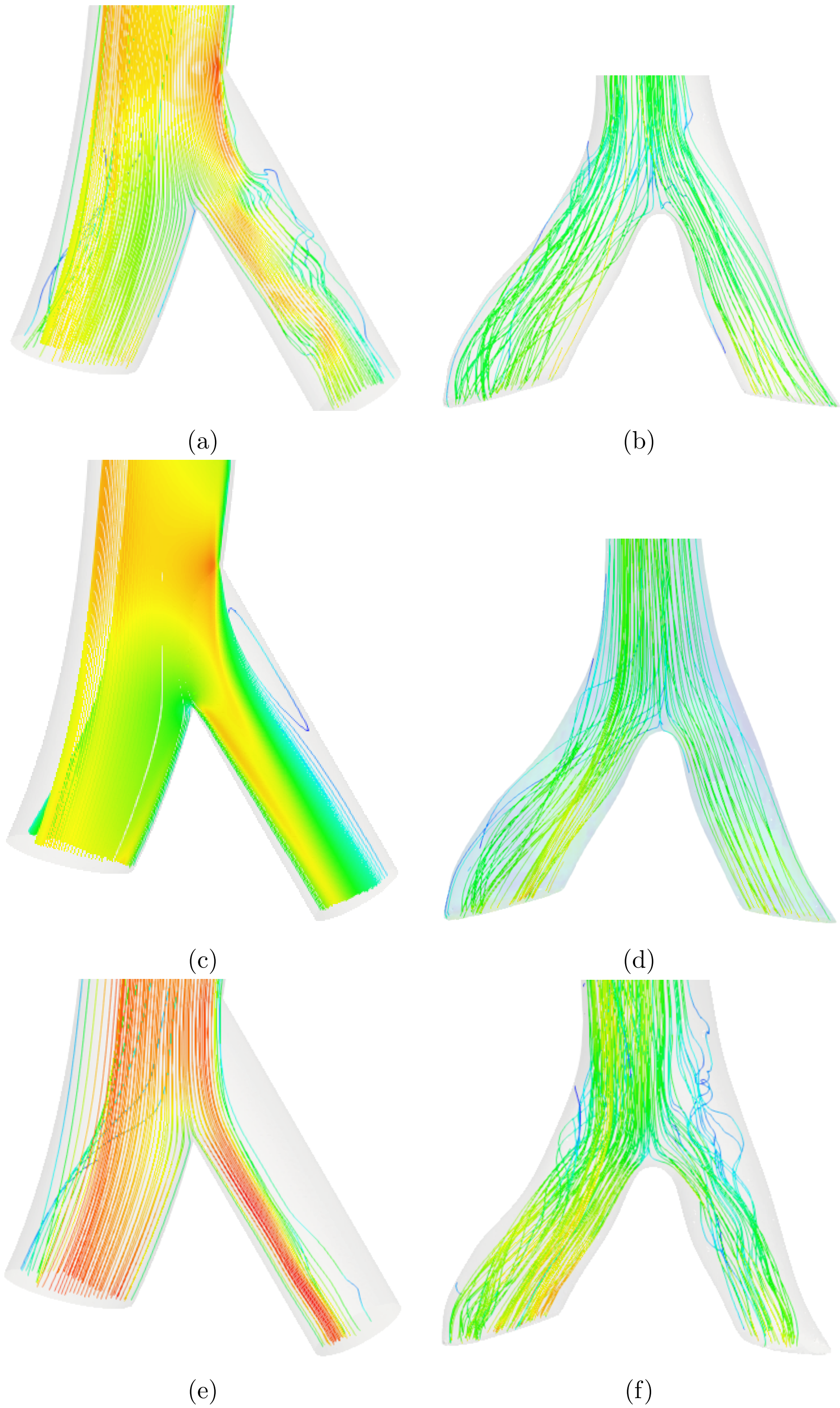

Figure 3.8. Comparison of the velocity streamlines obtained for both geometries: (a & b) Laminar , (c & d) $\kappa - \epsilon$, (e & f) LES.

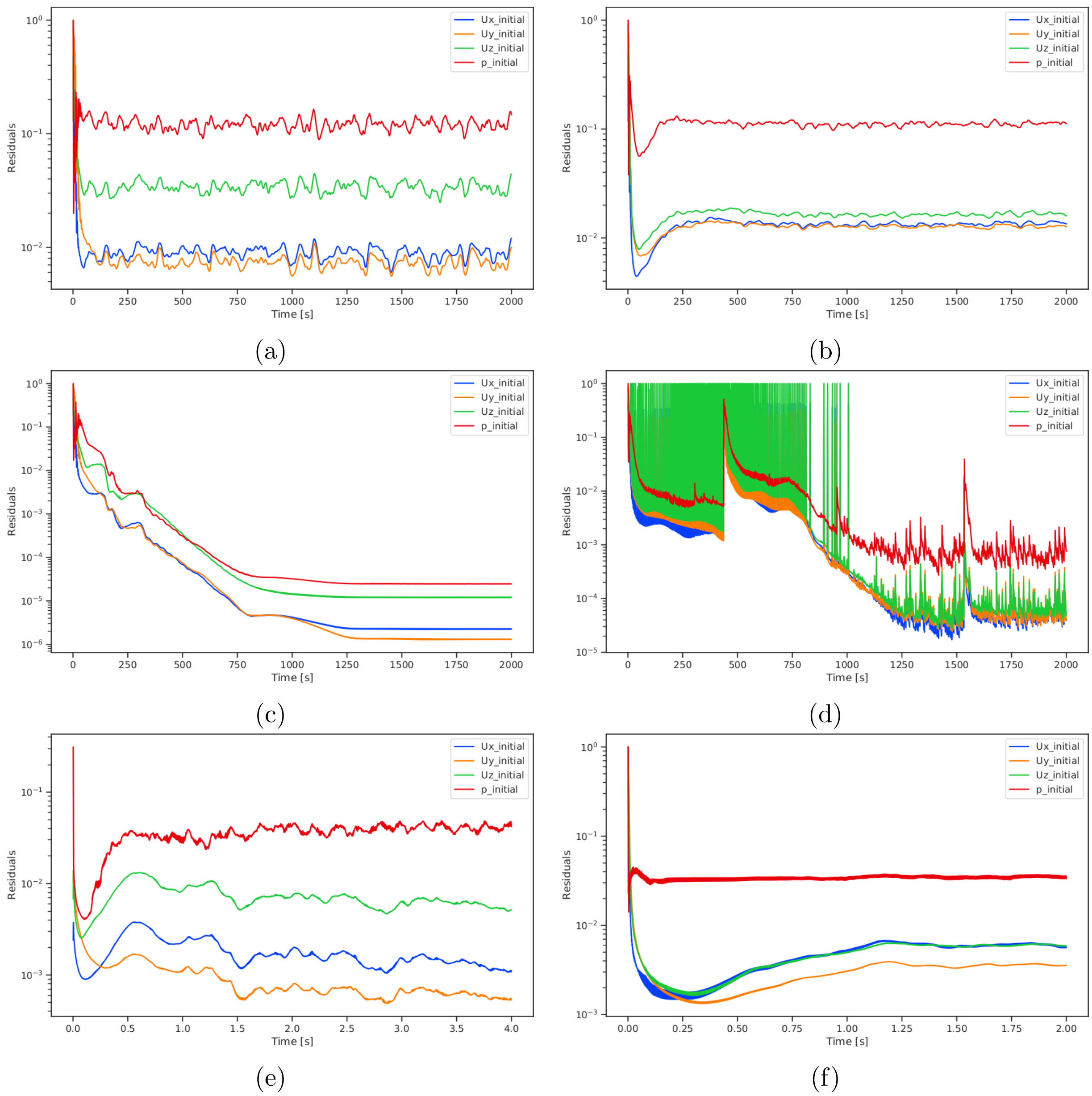

Figure 3.9. Initial residual historic obtained for both geometries: (a & b) Laminar , (c & d) $\kappa - \epsilon$, (e & f) LES.

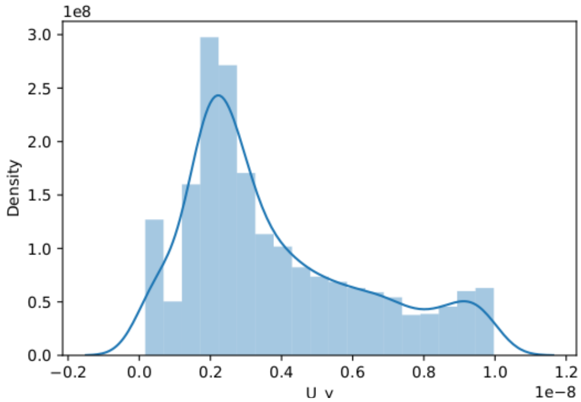

(a)

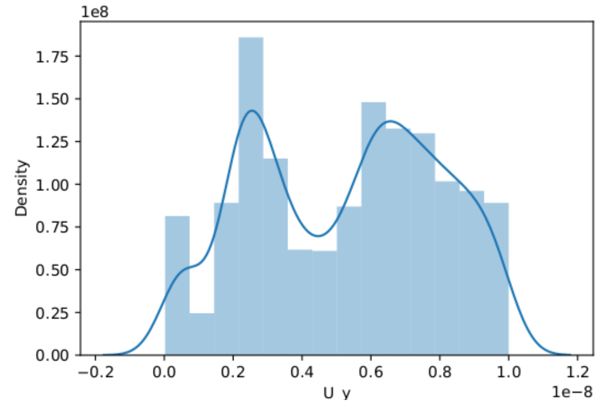

(b)

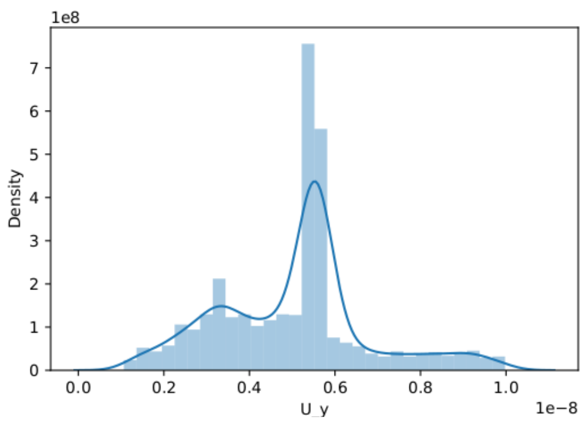

(c)

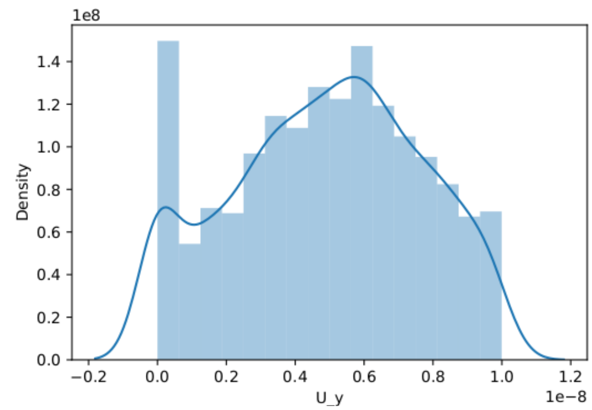

(d)

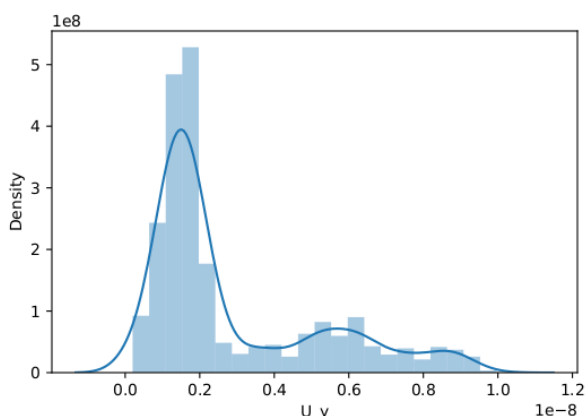

(e)

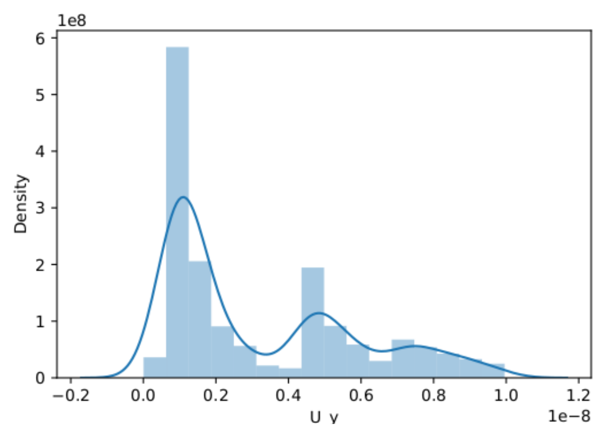

(f)

Figure 3.10. Histogram for Uy initial residual obtained for both geometries: (a & b) Laminar , (c & d) $\kappa - \epsilon$, (e & f) LES.

3.4 CONCLUSIONS

In this chapter, the velocity flow in the human upper airway was evaluated by comparing results obtained with different combinations of turbulence and geometry models. The results indicate that those two variables are closely related and can tremendously affect the veracity and detail of the viscous-flow computations, as well as particle deposition predictions.

One very distinct difference between turbulence models is the evidence of significant eddy formation captured using the LES model, as well as higher velocity values and overall, a more stable behavior from the variable's residuals. Furthermore, there is flow separation evidence under all turbulence models, however, the variable is highly dependent of the geometry, since shaped features in the idealized geometry resulted in stagnation points and completely different streamlines. The study suggests the combination of a more realistic geometry model combined with the LES turbulence model (at least for the boundary and flow conditions here considered), as the most effective on modelling the transitional/turbulent flow in the human upper airway. While it is true that flow pattern is very important in determining the deposition of particles, the streamlines presented here are only a rough estimation.

This research is merely a first step for considering more advanced physics and mathematics towards an adequate, practical and useful modeling of the breathing dynamics with the ultimate goal of a computational tool able to assist for the design of artificial respiratory devices and aids.

Chapter 4

Contact Problems for Linear Elastic Solids

4.1 MATHEMATICAL MODEL

The mathematical models presented previously and henceforward are to be discretised using the cell-centered Finite Volume Method, (FVM). As the reader probably knows, the Finite Element Method, (FEM), is dominant as numerical analysis technique in the field of computational solid mechanics (CSM), whereas the FVM has gained popularity among the computational fluid dynamics (CFD) problems. Both methods provide a discrete approximation of the exact integral equations, however, unlike standard FEM, where the strong form of the governing equation is cast into its equivalent weak form before discretization, the FVM directly discretises the strong integral form of the governing equations. The solids4Foam toolbox was built on the OpenFOAM software framework in a attempt for implementing object-oriented code to deal with combination of different solid and fluid procedures for FSI problems, (Cardiff et al., 2018).

The algorithm for the segregated linear geometry numerical implementation is shown next. Consists of a segregated algorithm where a loop is performed over the momentum equation solved for displacement, the loop will execute each time-step until convergence is achieved, resulting in an overall method that is implicit in time.

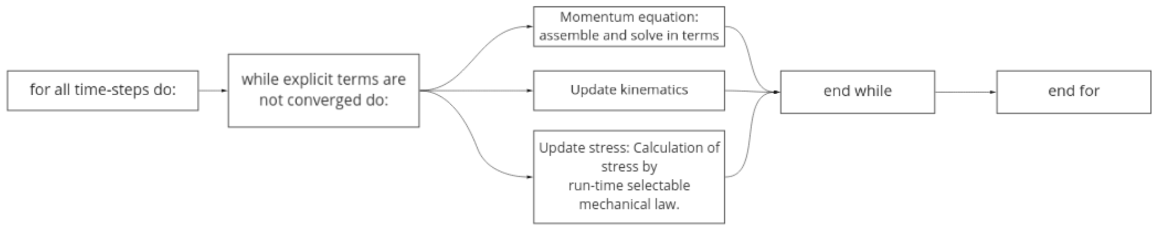

Figure 4.1. Algorithm for segregated linear geometry numerical implementation.

4.1.1 GOVERNING EQUATIONS

Tissue deformation in the solids is initially assume to behave linear elastic governed by Equation 4.1.

$$\frac{\partial \sigma_{ij}^{s}}{\partial x_j} + F_i = \rho \frac{\partial^2 D_i}{\partial t^2} \tag{4.1}$$

Where F_i is the body forces, D_i is the structural displacement, σ_{ij}^{s} is the solid stress tensor, and t is time. Moreover, the Cauchy stress tensor in the structural field is defined as in Equation 4.2, where E is the Young's modulus, ν is the Poisson ratio, ε_{ij} is the strain tensor.

$$\sigma_{ij}^{s} = \frac{E\nu}{(1+\nu)(1-2\nu)} \varepsilon_{kk} \delta_{ij} + \frac{E}{(1+\nu)} \varepsilon_{ij} \tag{4.2}$$

The deformations (strains/rotations) are expected to be "small": this means we can use a small strain approach, where the displacements are assumed not to affect the material geometry. In the case of linear geometry, the linearised strain tensor is defined in terms of the displacement gradient, as in Equation 4.3. And the deviatoric component can be seen in Equation 4.4.

$$\epsilon = symm(\nabla D) \;\; = \frac{1}{2}(\nabla D + \nabla D^T) \tag{4.3}$$

$$e = dev(\epsilon) = \epsilon - \frac{1}{3} tr(\epsilon)\mathbf{I} \tag{4.4}$$

The constitutive law for linear (Hookean) elastic materials is given by Equation 6.3, alternatively, as in Equations 4.5 and 4.6; three mechanical properties must be specified: Elastic/Young's modulus (E), Poisson's ratio (ν) and density (ρ). For this type of model, the momentum equation becomes a linear function of the displacement field D. However, a non-linearity is introduced through the contact boundary condition, that will be addressed later on.

$$\sigma^s = 2\mu\epsilon + \lambda tr(\epsilon)\mathbf{I} \tag{4.5}$$

$$\sigma^s = 2\mu\epsilon + \kappa tr(\epsilon)\mathbf{I} \tag{4.6}$$

The impenetrability contact constraints state that: (i) $d_N \geq 0$, i.e. no penetration may occur; d_N is the normal distance to the opposite contact surface and is negative for a point that crosses over the opposite contact surface, (ii) $t_N \leq 0$, i.e. the contact normal traction should be compressive or the contact surfaces cannot withstand tensile forces, and (iii) $t_N \cdot d_N = 0$, the complementary condition, i.e. if there is no contact, then no compressive tractions can occur; alternatively, if there are no compressive stresses, the distance must be positive.

The contact methodology, implemented by Cardiff, Karac, and Ivankovic (2014) in the OpenFOAM software is derived from the penalty method commonly used in finite element contact algorithms. It works by evaluating penetration of surfaces, namely: at the start of the analysis the two contacting surfaces are designated as the master and slave surfaces. During the iterative solution, the slave's vertices are checked for penetration of the master surface. If penetration does occur, an interface force is applied between the slave vertex, and the master surface, in the direction of the slave's normal, with magnitude proportional to the amount of penetration. Calculated slave vertex forces are then interpolated to the slave boundary face centres and applied as the traction boundary condition. If the analysis involves a deformable master body, the slave face tractions are interpolated to the master faces using a strongly conservative General Grid Interface interpolation method. For the rigid master body, however, the master surface is set to traction free. On this case-study, the master surfaces to study, will be assumed deformable. Finally, as the linear momentum equation is iteratively solved for displacement, the contact boundary updating procedure is repeatedly invoked. The specifics about immplementing the toolbox for this type of problem will be adressed later in Appendix B., where a step-by-step explanation of the basic toolbox functioning takes place; taking as reference the next case-scenario, Section **??**, which constitues an existing tutorial case on the solid contact in the OpenFOAM environment.

4.2 NUMERICAL IMPLEMENTATION - PUNCH CASE

Continuing with the hierarchical approach for understanding the problem and setting up the simulations the author first would like to introduce a benchmark type problem in order to explain and demonstrate how the OpenFOAM software and the solids4Foam toolkit approach solid mechanics and fluid solid interaction simulations.

In this case, a flat punch with rounded edges is presented into a flat-topped cylinder (Cardiff et al., 2018). The case demonstrates a three-dimensional quasi-static contact analysis of different materials; it is simulated with symmetries for demonstrative purposes. The problem geometry, shown in Figure 4.2, consists of a cylindrical punch with radius 50 mm and a 10 mm filleted edge, in contact with a flat-topped cylinder of 100 mm radius. The geometry was created using open-source software FreeCAD and exported in the IGES format to the open-source Gmsh software to create a facetted STL surface file; subsequently, a Cartesian mesh has been created using the OpenFOAM meshing utility cfMesh.

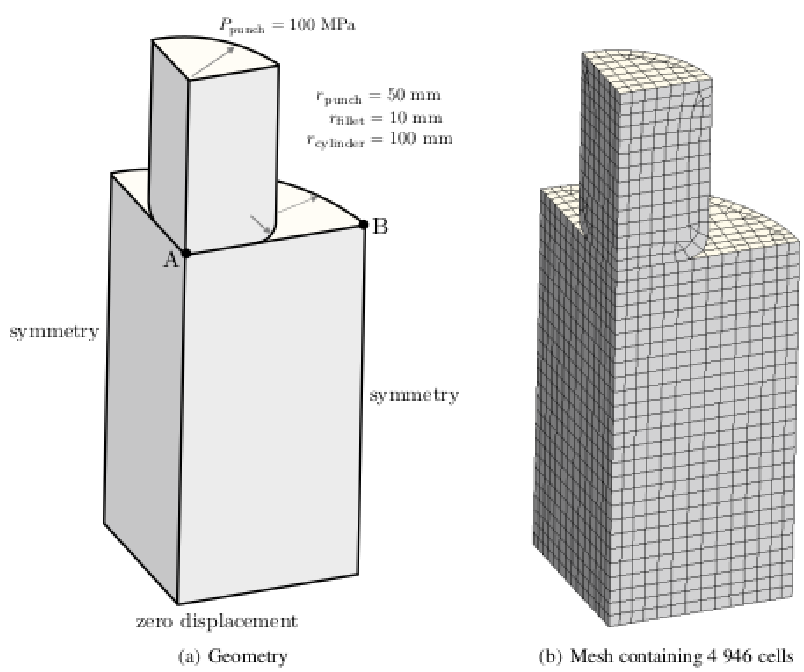

Figure 4.2. 3D Elastic punch. Problem geometry and mesh. Taken from (Cardiff et al., 2018).

A pressure of 100 MPa is applied to the upper surface of the punch, and the lower surface of the cylinder is fixed i.e. displacement is zero; in addition, two symmetry plane conditions are employed. To enforce the contact constraint conditions between the punch and cylinder surfaces, a penalty formulation,(commonly used in finite element contact algorithms), is employed for both the normal and friction models.

The punch is assumed to be steel and the cylinder is assumed to be aluminium, where the mechanical properties are given in Table 4.1.

Punch		
Young's modulus	E	$210GPa$
Poisson's ratio	ν	0.3
Cylinder		
Young's modulus	E	$70GPa$
Poisson's ratio	ν	0.3

Table 4.1. Elastic punch: Mechanical properties

The case is solved in one static time-step where inertia and gravity terms are neglected. A linear equation under-relaxation factor of 0.999 is used to ensure convergence; the use of equation (as opposed to field) under-relaxation has been found to be important in contact analyses, (Cardiff et al., 2018). The predicted axial and radial displacement distribution is shown in Figure 4.3. The contact pressure distribution can be seen from Figure 4.4.

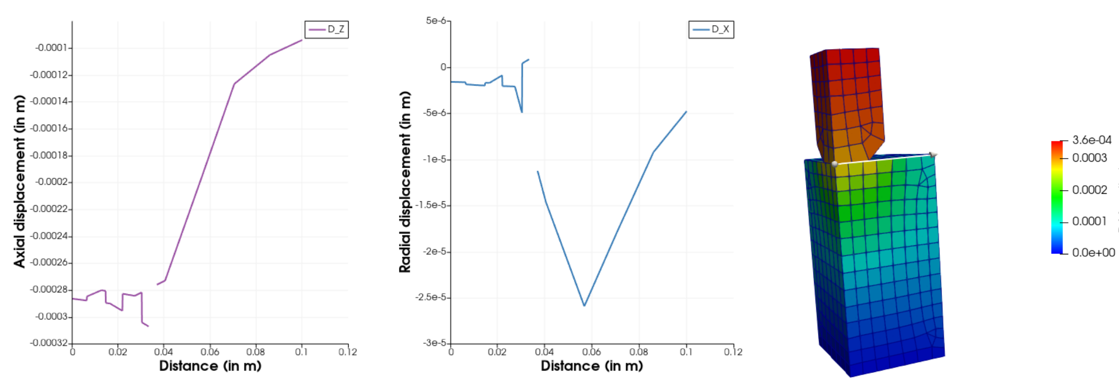

(a) (b) (c)

Figure 4.3. (a) Axial displacement along line. & (b) Radial displacement along line. & (c) Displacement magnitude contour.

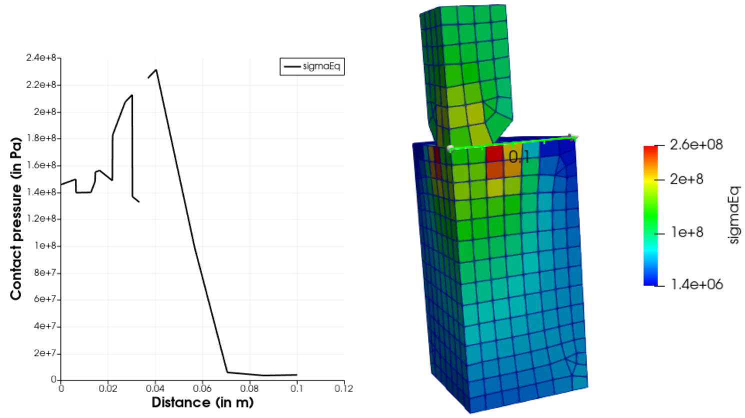

(a) (b)

Figure 4.4. (a) Von Mises stress distribution along line. & (b) Von Mises stress (equivalent sigma) distribution.

4.3 IDEALIZED ENDOTRACHEAL CUFF - METODOLOGY

Following the previous case-scenario and the contact boundary condition, it is relevant to get back to the track of the investigation continuing with the case were the author is interested in obtaining the stresses and displacements generated in the contact problem between an endotracheal cuff and the air-wall that is the trachea, (idealized versions of both). Again dealing with $3D$ quasi-static contact analysis of different materials.

One expects the cuff to deform due to the internal applied pressure (that attempts to resemble the process of inflation when intubating patients), consequently, the air-wall will be under deformation and stress. The problem geometry, shown in Figure 4.5 (a), consists of an spherical shaped cuff of $191mm$ outer diameter and thickness of $2mm$, in contact with a cylindrical tube with $217mm$ outer diameter and $3mm$ thickness. The geometry has been created using the Fusion360 software from AutoDesk and exported to STL faceted surface files; then, the meshing process is conducted using the OpenFOAM meshing utility *snappyHexMesh*. To do so, one must first define a "enclosure mesh", which is done with *BlockMesh*, that one needs to consist on purely hexahedra elements and it is used to further refine the mesh on the snapping process. It can be seen on Figure 4.5 (b), and has 129600 cells.

After obtaining the background mesh one can operate with the *snappyHexMesh* utility, where three steps are conducted as the stages of the meshing process: first, cell splitting is performed according to specified edge features. Second, a process of cell removal begins, where depending on the application (if it is external or internal flow phenomena), removes cells inside or outside

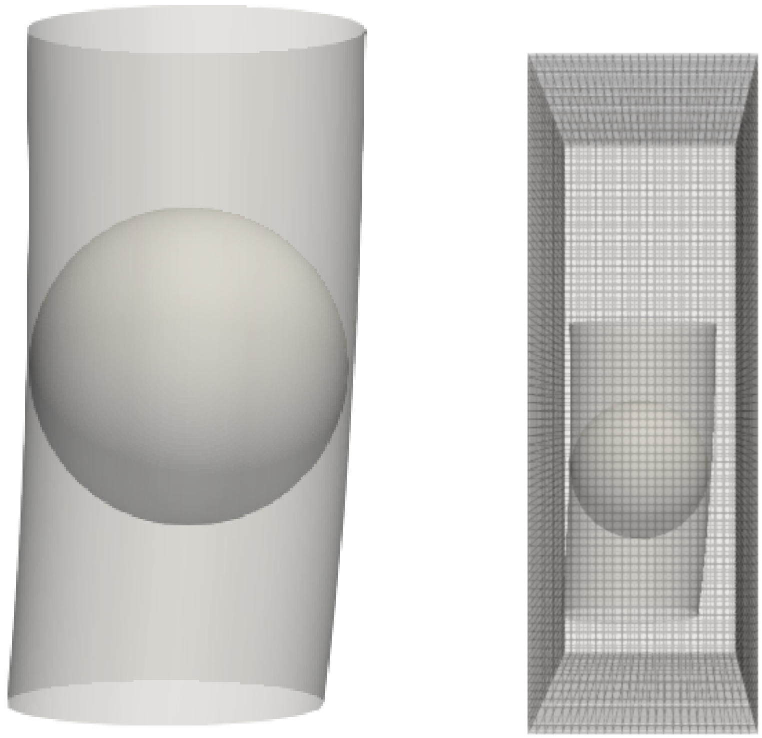

(a) (b)

Figure 4.5. (a) Idealized cuff geometry generated in STL format & (b) Background mesh obtained with BlockMesh utility.

the splitted cells. Thrid, snapping to surfaces, which implies moving cell vertex points onto surface geometry to remove the jagged castellated surface from the mesh. Additionally, even though the mesh output from the snapping stage may be suitable for the purpose, it can produce some irregular cells along boundary surfaces. There is an optional stage of the meshing process which introduces additional layers of hexahedral cells aligned to the boundary surface (Greenshields, 2018). It is a sufficiently robust and flexible utility for meshing if the user is interested and willing to interact with parameters involved in a command-like manner.

The resulting mesh from this stage is shown in Figure 4.6 (a). It consist of 2744217 cells, where most of them are hexahedra, however there is also presence of polyhedra-type cells; as explained by Cardiff et al. (2018), in contrast to standard FEM, where shape functions are specific to the shape of the element, in the current cell-centred FVM no distinction is made between different cell volume shapes, as all general polyhedra (for example, tetrahedra, hexahedra, triangular prism, dodecahedra, etc.) are discretised in the same general fashion.

Some parameters, for example the maximum aspect ratio being 5.41, the maximum skewness 3.3 and the average mesh non-orthogonality of 13.8, can be translated into a proper mesh quality that passes the standard OpenFOAM mesh quality check.

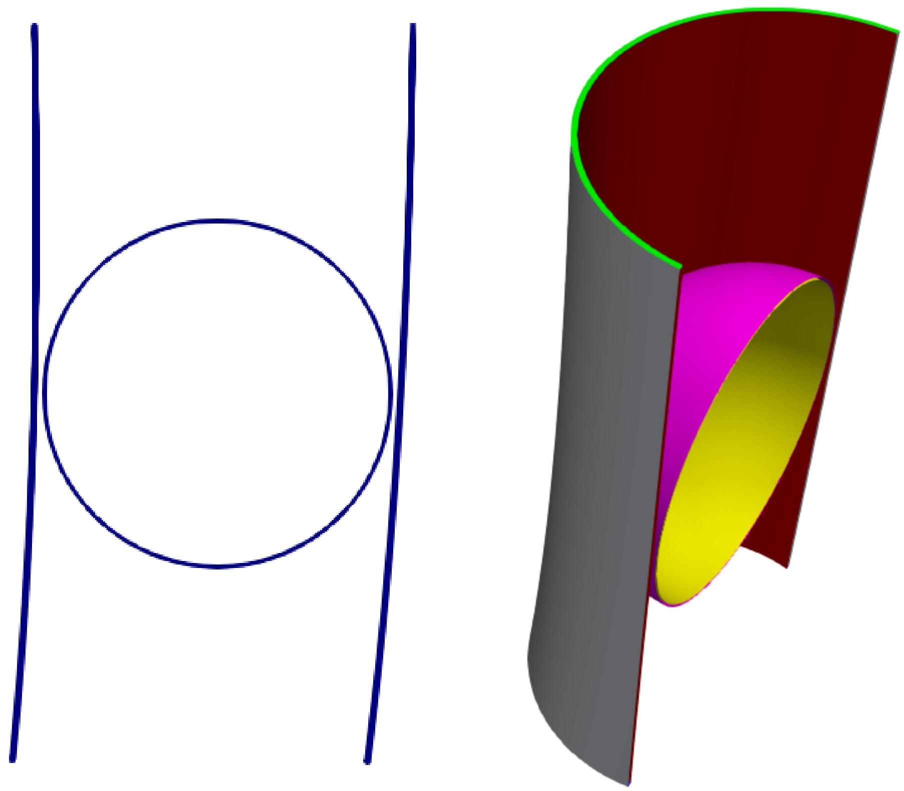

(a) (b)

Figure 4.6. Mesh generated usign snappyHexMesh utility. (a) Cut section of internal mesh & (b) Patches in mesh

As seen in Figure 4.6 (b), each color represents a different patch. The mesh (initially consisted of only the sphere and cylinder) had to be manipulated with some OpenFOAM utilities in order to separte the patches for accurately impose the boundary conditions of the problem. This manipulation can be explored in more detail on Appendix B..

4.3.1 BOUNDARY CONDITIONS

Tracheal tissue is modelled as homogeneous and isotropic which seems to be fair for first studies. For cartilage, fitting the experimental curves to an elastic model, a Young's modulus of $3.33MPa$ is assumed based on the work by Trabelsi, del Palomar, López-villalobos, Ginel,

Trachea section		
Young's modulus	E	$3.33MPa$
Poisson's ratio	ν	0.49
Endotracheal cuff		
Young's modulus	E	$1MPa$
Poisson's ratio	ν	0.28

Table 4.2. Idealized cuff contact: Mechanical properties

and Doblaré (2010), where mechanical tests and histological analyses are used to characterize the tissues. A Poisson ratio of as 0.49 is used, based on the fact that most biological tissues are considered as roughly incompressible materials according to Liu et al. (2018), were that parameter value was obtained from published porcine cadaver experimental data in previous investigations. The endotracheal cuff introduced here as a polymeric surface is assumed to be elastic material with Young modulus of $1MPa$ and Poisson ratio of 0.28, following the research of Malvè et al. (2010). Mechanical properties are found on Table 4.2.

In vivo boundary conditions are often very hard to specify or measure. Therefore, the employed boundary conditions are sometimes non-physiological for this initial study. Nevertheless, the adopted model will allow helpful insights. The air-tissue interface was allowed to deform whereas the other wall regions (inlet and outlet, i.e. top and bottom of the tracheal section) were assumed rigid. To enforce the contact constraint conditions between the sphere and cylinder surfaces, a penalty formulation is employed for both the normal and friction models.

On this study case, the numerical boundaries conditions used are different in each mesh patch, as mentioned before. Let's examine that in further detail:

- At the "inlet" and "outlet", meaning, the green line in Figure 4.6 (b), and its bottom similar, the BC is *fixedDisplacement*, in order to mimic the real behavior of the trachea inside the toraxic cage.
- For the inner cylinder, seen in red on Figure 4.6 (b), the contact boundary condition was applied, being this patch the master in the definition of the BC functioning explained in the mathematical model. The BC is *solidContact* in solids4Foam environment.
- The outer cylinder, seen in grey on Figure 4.6, (b) is free to deform under the *solidTraction* condition.
- The outer sphere, (fusia in the Figure) is the contact slave on this analysis, since that

is the one to stablish contact with the cylinder. The boundary conditions on that case is the same, however its parameters in the solids4Foam IC's vary according to its slave condition.

- The inner-yellowy sphere, is under an IC of *solidTraction*, but with an assigned time-dependent pressure value of 0.001471 Mpa at 5 seconds, corresponding to 15 cmH20. This to simulate the process at which the endotracheal cuff is inflated at the mechanical ventilation procedure.

The three dimensional domain is represented by $(\Omega_1 \& \Omega_2) \subset \mathbf{R}^3$. And the domain boundary consist of $\partial\Omega_1 = \partial\Omega_{InnerCyl}, \cup\partial\Omega_{OuterCyl}, \cup\partial\Omega_{in}\cup\partial\Omega_{out}$, and $\partial\Omega_2 = \cup\partial\Omega_{InnerSph}, \cup\partial\Omega_{OuterSph}$, where they represent the patches from the cylinder and sphere geometries. Here, the displacements and tractions on the boundary are defined as in Figure 4.7.

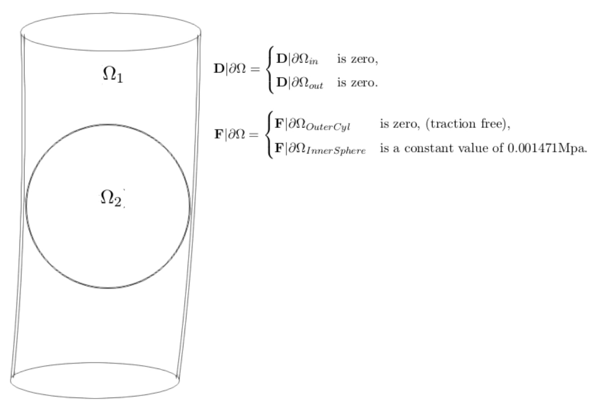

Figure 4.7. Schematic of boundary conditions used for initial solids contact simulations.

4.3.2 NUMERICAL SCHEMES

The numerical schemes have been chosen, according to mesh quality, following instructions and suggestions provided by the solids4Foam documentation. The schemes are collected in the Table 4.3.

4.3.3 SOLVER EXECUTION

In OpenFOAM, the equation solvers, tolerances, and algorithms are controlled from the sub-dictionary **solvers** located in the *fvSolution* dictionary file, the **solvers** sub-dictionary specifies each linear-solver that is used for each equation being solved; The syntax for each entry

Numerical schemes	
d2dt2Schemes	Euler
ddtSchemes	Euler
gradSchemes	extendedLeastSquares 0
divSchemes	Gauss linear
laplacianSchemes	Gauss linear corrected
interpolationSchemes	linear corrected
snGradSchemes	corrected

Table 4.3. Numerical schemes Table for solids contact case.

uses a keyword that is the word relating to the variable being solved in the particular equation and the options related to the linear-solver.

The displacement equation is very similar to the pressure one, in standard CFD approaches, (both varables have simmetric matrices); as such, the conjugate gradient (PCG) or the algebraic multi-grid (GAMG) linear solvers tend to work best. On this research, the **PCG** method, (Newton-Krylov solver) was chosen with the FDIC preconditioner.The solver tolerance can be set 0.1 as outer iterations are performed over the momentum equation until convergence.

A second sub-dictionary of fvSolution that is often used in OpenFOAM is relaxation factors which controls under-relaxation, a technique used for improving stability of a computation, particularly in solving steady-state problems. Under-relaxation works by limiting the amount which a variable changes from one iteration to the next, either by modifying the solution matrix and source prior to solving for a field or by modifying the field directly (Guerrero, 2019). An optimum choice for this values are the ones small enough to ensure stable computation but large enough to move the iterative process forward quickly. Moreover, in general, the D equation and field do not requires under-relaxation; however, in contact analysis equation relaxation can help, in this study the relaxation of the D equation is set to 0.999, since relaxation factors less than 0.1 would be result in prohibitively slow solution procedures.

Part III

Epilogue

Chapter 5

Epilogue

5.1 CONCLUSIONS AND FURTHER WORK

5.1.1 CONCLUSIONS

This thesis proposed a framework for the analysis of fluid-dynamics and solid mechanics with the finite volume method in the context of breathing phenomena, with particular interest in mechanical breathing processes. To do so, this thesis included the synthesis between: a decent state of the art of relevant researches on the computational modeling of breathing, the implementation of the FVM in OpenFOAM's environment, and a brief theoretical annex in FSI theory.

The problem was approached first by considering the fluid's behavior when changing geometries and turbulence models. Two different geometries were investigated, they attempted to resemble part of the human trachea; the first geometry consisting on cylindrical tubes, and the second based on a CT scan reproduction. Both geometries were tested with the laminar, $\kappa - \epsilon$, and LES models. A very simple flow of $2.3m/s$ was simulated and analyzed. This part of the investigation reaffirmed that the results of such simulations is greatly affected by the combinations chosen between geometry and turbulence modeling. The main result of this part of the book consisted of a graphical representation of the flow field values and streamline patterns in all the studied conditions; as well as residual plots. The results were also contrasted with histogram plots and the comparison between statistical behavior of data when changing the variables. Available Python code was generated to evaluate differences in results when considering a laminar or turbulent model, and for the purpose of data visualization.

Once the fluid-dynamics point of view gave the author a deeper understanding of the problem, a solids contact framework problem was reproduced with the solids4Foam toolkit. At this point, notions of the OpenFOAM environment were employed, to gain as much relevant information as possible for next steps. The results of this approximation included the predicted displacements and stresses in a selected line, and helped the author in the pursuit of a better understanding of the FVM in solid mechanics, to finally enable them to establish a methodology of yet another solids contact problem, this time with idealized geometries more alike the ones involved in the mechanical ventilation procedure, (trachea and endotracheal cuff). Although the numerical results for this last part of the book are not presented, the expected results would reveal trends on axial displacements and Von Mises stress characteristics in the tracheal geometry when submitted to the cuff's inflation.

A theoretical analysis based on existing literature has been written in the fluid-structure interaction modeling, in hopes some curious and perhaps not very experienced reader, much like the author herself, can find a brief introduction to the subject. This was also done considering that to be the next step when attempting to model the aforementioned phenomena. Three different angle combinations were studied on this part; however, this would be enough to draw interesting conclusions. Finally, the reader will find Appendix on the turbulence modeling mathematical background and the specifics of solids4Foam usage for the cases on this thesis, also with the intention to serve as tutorials in case someone wishes to simulate contact problems on this toolkit.

The present study aimed to combine various tools to the study of breathing phenomena; the aim was to determine the possible modifications in the relative contribution of the geometry chose in different turbulence models, and set a precedent in literature for solids contact problems resolved by the FVM in OpenFOAM's environment. The authors are very pleased with the results pointed out in all sections of the thesis, since part of the challenge of carrying out this study was to be able to perform the required analyses, using resources and tools available in the UPB campus. By itself, this work feels like an important step towards sports science becoming a research topic of interest in Colombia.

5.1.2 FURTHER WORK

Since in this thesis, the variables were measured using idealized geometries, and this does not truly represent the complexity of phenomena involved in breathing and mechanical breathing, an inevitable pathway to further work is to assemble all the tools used into one cohesive analysis in which more realistic models are taken into account.

As mentioned before on this book, the particle deposition around the endotracheal cuff greatly increases the risk of acquiring pneumonia on mechanically ventilated patients; an study evaluating the efficiency of particle seal when varying between different designs of the aforementioned device is relevant when attempting a conscious study of mechanical breathing. This would enable more effective design processes for endotracheal cuffs, directly impacting on saving human lives. Besides this, a comprehensive and multi-physics modeling of the phenomena, such as the one found in Dailey and Ghadiali (2007) should be readjusted to the present context, including the fluid-structure interaction of the cuff's inflation and the particle transport and deposition phenomena occurring on the trachea when a patient is mechanically ventilated. That should constitute the last step towards a more accurate simulation of the real-life process.

Since time is limited in a research such as the one developed through the present book, these mentioned topics are left to be a future work of those researchers interested in the development of an out-of-the-box thinking, leading to new and exciting engineering applications. To paraphrase Marcus du Sautoy, the power of mathematics, is its ability to generalize results beyond their original context, and to find applications far beyond anything anyone might have expected; I believe it is the job and passion of the engineer to take advantage of scientific knowledge and modern computing technology to bring insights and innovate in day-to-day life phenomena.

Chapter 6

Annex - Appendix

6.1 FLUID STRUCTURE INTERACTION

Fluid-Structure Interaction (FSI) has encounter a growing interests within the scientific community, as the dynamical behavior of flexible structures in the presence of fluids comes into play in numerous industrial and scientific applications. The computation of FSI problems requires the solution of the coupled fluid and solid underlying governing equations (Wall & Rabczuk, 2008), and as the two sub problems are big mathematical challenges on their own, it is no surprise that results for the coupled problem are rarely spread.(Richter, 2017) Depending on the application or assumptions made each problem has different characteristics, leading to different dynamics of the coupled system and different demands to the describing models and to the computational approaches.

In this study we are interested in knowing the principal stresses and strains under which the trachea is submitted when the patient is under mechanical ventilation, because, as stated by Malvè et al. (2010), the trachea as a construction is a reinforced tube; sixteen to twenty cartilaginous half-rings whose ends are connected by a soft membranous wall form the anterior tracheal wall. Understanding the breathing process under forced ventilation in a trachea model, and how the airflow and stresses distribute in the airway wall is essential in order to design more convenient prostheses or mechanical ventilation techniques. It is also important for this research to quantify how the FSI influence particle deposition, as it is an undesired effect on mechanically ventilated patients.

6.1.1 KINEMATICS AND GOVERNING EQUATIONS

It is important to first understand the kinematic discussion of the problem, since, as stated by Luca Formaggia (2009), kinematics is the part of mechanics that describes the motion, forms the background that enables to derive the differential equations which translate fundamental principles of physics into mathematical terms. Fluid flow is usually developed under the Eulerian frame where kinematics is described in the current (deformed) configuration. The airflow under mechanical ventilation condition is governed by the incompressible continuity and Navier-Stokes equations.

$$\rho \frac{\partial u_i}{\partial x_i} = 0 \tag{6.1}$$

$$\rho \frac{\partial u_i}{\partial t} + \rho u_j \frac{\partial u_i}{\partial x_j} = -\frac{\partial p}{\partial x_i} + \mu \frac{\partial^2 u_i}{\partial x_j \partial x_j} \tag{6.2}$$

Where ρ is the fluid density, μ is the fluid viscosity, u_i is the velocity vector, x_i is the position vector, t is time, and p is the fluid pressure. Note that the equations are written in standard indicial notation. In the Eulerian formulation one observes what happens at a given point x_i, in the physical space. Here, large distortions in the continuum motion can be handled, but generally at the expense of precise interface definition and the resolution of flow details, (Donea, Huerta, Ponthot, & Rodriguez-Ferran, 2004). The Cauchy stress tensor in an isotropic Newtonian fluid is defined as in Equation 6.3.

$$\sigma_{ij}{}^{f} = -p\delta_{ij} + 2\mu\left(\varepsilon_{ij} - \frac{1}{3}\varepsilon_{kk}\delta_{ij}\right) \tag{6.3}$$

Where, $\sigma_{ij}{}^{f}$ is the fluid stress tensor, ε_{ij} is the rate of the strain tensor which is given by Equation 6.4.

$$\varepsilon_{ij} = \frac{1}{2}\left(\frac{\partial u_i}{\partial x_j} + \frac{\partial u_j}{\partial x_i}\right) \tag{6.4}$$

The Lagrangian frame describes kinematics in the reference configuration. This allows tracking of free surfaces and interfaces with relative ease; is therefore weaker to follow large distortions of the computational domain if one does not fall back on frequent re-meshing operations. Tissue deformation in the solid domain is initially assume to behave linear elastic governed by Equation 6.5.

$$\frac{\partial \sigma_{ij}^{s}}{\partial x_j} + F_i = \rho \frac{\partial^2 D_i}{\partial t^2} \tag{6.5}$$

Where F_i is the body forces, D_i is the structural displacement, σ_{ij}^{s} is the solid stress tensor, and t is time. Moreover, the Cauchy stress tensor in the structural field is defined as in Equation 6.6, where E is the Young's modulus, ν is the Poisson ratio, ε_{ij} is the strain tensor.

$$\sigma_{ij}^{s} = \frac{E\nu}{(1+\nu)(1-2\nu)}\varepsilon_{kk}\delta_{ij} + \frac{E}{(1+\nu)}\varepsilon_{ij} \tag{6.6}$$

The fundamental dilemma or modeling FSI, according to Richter (2010), is coupling two systems of partial differential equations that are given in two different coordinate systems. To do so, one has to impose a set of coupling conditions on the interface, were coordinates always must be mapped between the different systems. Therefore, the fluid-structure interaction is achieved by satisfying either a velocity or displacement continuity, as in Equation 6.7, and the force equilibrium across the FSI interface, as in Equation 6.8, where n_i is the normal vector outward of the FSI interface; D_i^f and D_i^s are the fluid and solid nodal displacements.

$$n_i u_i = n_i \frac{\partial D_i}{\partial t} \tag{6.7}$$

$$n_i \sigma_{ij}^{f} = -n_i \sigma_{ij}^{s} \tag{6.8}$$

$$D_i^f = D_i^s \tag{6.9}$$

As explained by Dailey and Ghadiali (2007), the **kinematic condition** of Equation 6.7 requires equal fluid and solid nodal velocities on the moving fluid-solid boundary; it also acts as a *no slip* condition for the fluid's velocity on the interface. The **dynamic condition** in Equation 6.8 specifies stress continuity between the fluid and solid domains; this reflects the *Neumann-condition* for the normal stresses that drives the solid problem. Finally, the **geometric condition** in Equation 6.9 requires equal displacements of the fluid and solid stress tensors. The geometric condition takes a special role, it does not reflect a physical material principle but deals with the domain partitioning (Richter, 2010). In these equations, the left-hand side represents the fluid's state, and the right-hand side the state of the structure. See Figure 6.1

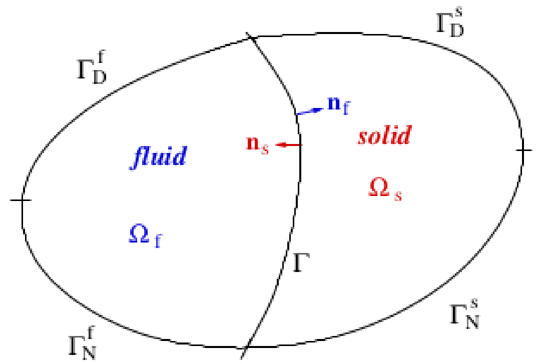

Figure 6.1. Coupling conditions on fluid-structure interaction.

6.1.2 ARBITRARY LAGRANGIAN EULERIAN FRAMEWORK

As mentioned earlier, FSI problems require the solution of **coupled** fluid and solid governing equations. Talking about **coupling** implies a system in which different components interact **dynamically** and, as mentioned by Felippa et al. (2001), the physical interaction is *multi-way*. On this case-study for instance, motion of the solid air-way due to the endotracheal cuff inflation changes the geometry and therefore the fluid domain, this is the **geometric condition**. Then, the attached fluid moves, **kinematic condition**. And finally, change of the fluid-domain results on a flow field alteration, hence generating new (different) forces on the trachea wall, **dynamic condition**. See Figure 6.2. Those three principles (geometric, kinematic and dynamic conditions) mainly determine the dynamics of the coupled problem (Richter, 2017).

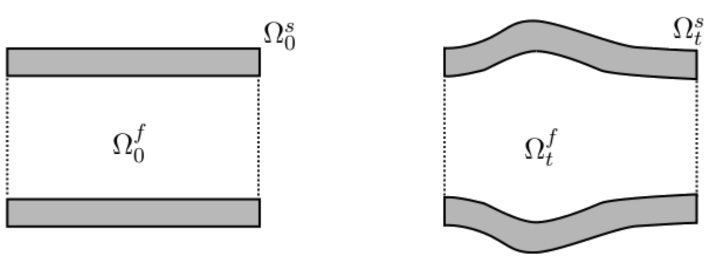

Figure 6.2. The computational domain Ω^f for the fluid in a section of the trachea. It deforms to follow the air wall movement once the endotracheal cuff is inflated, yet the axial position of its proximal and distal boundary is kept fixed. Its evolution is described by the ALE map

Evidently, the need of dealing with equations on moving domains comes as one of the major challenges of numerically proposing the physical FSI, besides the fact that motion is not prescribed but an additional unknown of the problem. As explained by Richter (2017), moving domains are typical in structure mechanics, since the movement of the solid is exactly the unknown solution. The solid's description of motion is usually reproduced (numerically) in a way were each individual node of the computational mesh follows the associated material particle during motion Donea et al. (2004). However, in fluid-dynamics a fixed domain is usually set, were the continuum moves with respect to the grid. With the aim of combining advantages and minimizing shortcomings of pure Lagrangian and Eulerian algorithms, the ***Arbitrary Lagangian Eulerian*** (ALE) technique has been introduced and developed since the 1970s. Here, a reference domain (called *arbitrary*) is set as somewhere in between the Eulerian and Lagrangian systems, and a mapping between this referential, the material and spatial domains is conducted. Therefore, as explained by Donea et al. (2004) the nodes of the computational mesh may be moved with the continuum in normal Lagrangian fashion, be held fixed in Eulerian manner, or be moved in some arbitrarily specified way to give a continuous rezoning capability. This enables the ALE description to accommodate significant distortions of the computational mesh, while preserving the clear delineation of interfaces.

In an ALE framework, the mesh velocity $\tilde{u}_i$ becomes an additional nodal unknown which is subtracted from the material velocity u_i. They both have been defined by deriving the equations of material motion and mesh motion respectively with respect to time, (**?**). There is also the "particle velocity",which measures the time variation of the referential coordinate holding the fixed material particle. The relation between these velocities yields the convective velocity c_i, that is, as explained by Donea et al. (2004), the relative velocity between the material and the mesh. Since it would be very difficult to specify grid velocity for the current problem, the practical implementation of the ALE description requires an automatic mesh-movement algorithm.

The ALE differential and integral forms of the conservation equations are the basis for the spatial discretization for numerically solving problems involving fluid dynamics and solid mechanics. There is a fundamental ALE relation between material time derivatives, referential time derivatives, and spatial gradient but such an expression and its derivation is beyond the aim of this article. To obtain the ALE form of the conservation equations all one has to do is replace in the various convective terms, the material velocity u_i with the convective velocity $c_i = u_i - \tilde{u}_i$, as in the ALE mass conservation in Equation 6.10 and the ALE momentum in Equation 6.11. The right-hand side of those is written in classical Eulerian fashion (spatial domain), similarly to Equations 6.1 and 6.2. The left-hand side however, reflects the arbitrary motion of the computational mesh, (referential domain), here denoted by χ.

$$\left.\frac{\partial \rho}{\partial t}\right|_{\chi} + c_i \cdot \nabla \rho = -\rho \nabla \cdot u_i \tag{6.10}$$

$$\rho\left(\left.\frac{\partial u_i}{\partial t}\right|_{\chi} + \left(c_i \cdot \nabla\right) u_i\right) = \nabla \cdot \sigma + \rho f_i \tag{6.11}$$

In general, $u_i \neq \tilde{u}_i$, however, we can note two particular cases:

- If $\tilde{u}_i = u_i \longrightarrow c_i = 0$ then the mesh description would be Lagrangian;
- If $\tilde{u}_i = 0 \longrightarrow c_i = u_i$, the computational domain is fixed for all times and in that case the description would be Eulerian.

Additionally, as explained by Margolin (1997), the three phases of an ALE simulation, as described by Hirt et al., are: an explicit Lagrangian update, an implicit iteration of the momentum equation with the equation of state, and a rezone/map phase. The Lagrangian phase provides an explicit update of the equations of motion. Finally, a rezone algorithm may prescribe mesh velocities relative to the fluid, thus necessitating a remap phase in which the solution from the end of phase two is mapped onto the new mesh. Moreover, a particularly important property of ALE is that it provides a means of minimizing advection errors.

6.1.3 SPACE DISCRETIZATION OF THE COUPLING CONDITIONS

Various numerical problems appear when considering the modeling and simulation of coupled systems as it is the fluid-structure interaction. In this sense, we have a problem to solve, and there is mainly three different ways to approach it: monolithic, partitioned and others in between. We refer to a *Monolithic* scheme when trying to solve the problem all at once; it is treated as a monolithic entity and all components advance simultaneously in time. This approach is typically *strongly coupled*, meaning that the coupling conditions on Equations 6.7, 6.8 and 6.9 are satisfied after time discretization (Luca Formaggia, 2009).

However, it is from many centuries of experience that science has understood that probably the most efficient way to tackle a complex system or situation is by breaking it down into smaller, more manageable pieces. This reasoning goes as far as the very foundation of calculus when they first attempted to measure the area of a circle by breaking the curve into many small rect segments, and that is the same reasoning behind the *Partitioned* approach or scheme. The term *partitioning* refers to the *spatial* separation of a discrete model into interacting components generically called *partitions* (Felippa et al., 2001). The decomposition can be chosen according to specific objectives, for example, the structure that represents the human upper airway can be decomposed according to function into substructures as nose, pharynx, trachea. Substructures can be further decomposed into sub-meshes or subdomains as the fluid's domain of the air and particles passing trough the solid's domain that represents the trachea air-wall. Subdomains con be further decomposed into individual elements.

In terms of the software engineering aspect, partitioned approaches for the simulation of multi-physics scenarios offer a great potential: They reuse existing, established, tested, and trusted codes for single-physics problems and couple them to a multi-physics simulation environment via suitable software tools and numerical coupling strategies (Hans-Joachim Bungartz, 2010). When the fluid and the solid are solved with their own software the capabilities of evolution and optimization of each code increase greatly. This advantages, of course, does not come for free but raises the new challenge of developing numerical coupling strategies that yield stable transient coupled simulations. First to consider, a partitioned scheme is not necessarily weakly coupled: when sub-iterations are performed at each time step, the coupling conditions aforementioned can be enforced with a high accuracy even though two different solvers are used. Nevertheless, partitioned procedures are often used to implement weakly coupled schemes (Luca Formaggia, 2009). Second, another numerical aspect that has to be kept in mind -in particular with respect to physical conservation laws- is the mapping of data between the in general non-matching solver grids.

A simple loosely coupled partitioned FSI algorithm, as explained in Rasani et al. (2011) could consist on a successive iteration where the fluid variables are solved based on the initial geometrical configuration (Dirichlet boundary conditions). The fluid pressure and shear forces at the elastic segment are interpolated to the nodes on the elastic wall. Applying them together with the external pressure and imposed boundary conditions (Neumann BC's), the solid solver solves for the deformation of the elastic wall. These nodal deflections are then interpolated back to nodes on the elastic boundary of the fluid, which is used to effect the mesh deformation on the fluid domain. The fluid solver then solves the unknown fluid variables using the current geometrical configuration and the process is repeated until the nodal deflection and forces in the coupling conditions from current and previous coupling iterations are within a specified tolerance, because, to maintain stability and to speed the approach to convergence, the solver employs displacement and stress relaxation factors when passing boundary information between the fluid and solid domains. When the solver reaches a converged solution, it stores the information and moves to the next time step. The overall process can be summarized as in Figure 6.3

Furthermore, as explained by Felippa et al. (2001), partitioning may be algebraic or differential. Here we attempt to explore the differential approach, were the decomposition is done

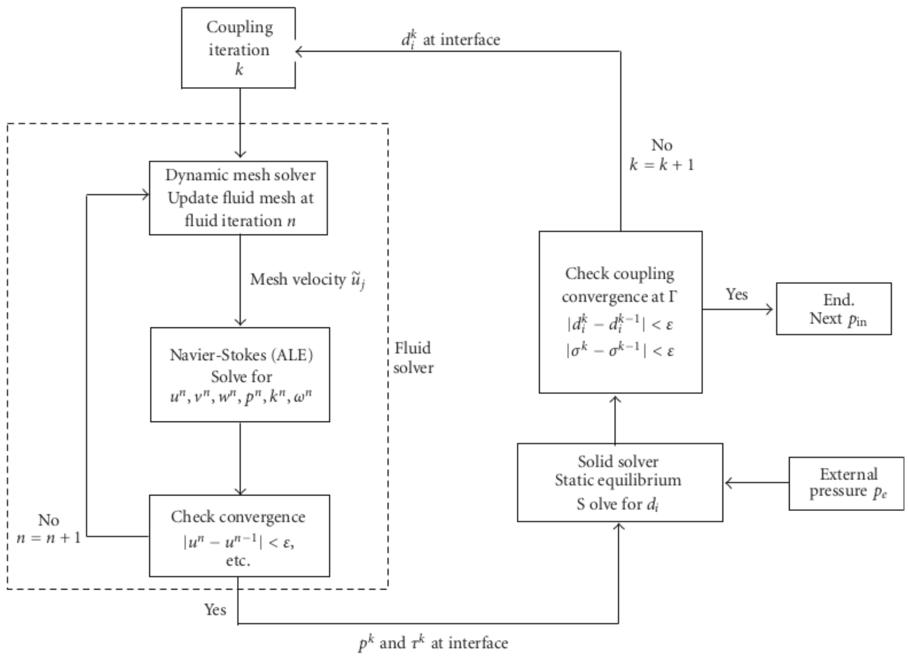

Figure 6.3. FSI flow chart, taken from Rasani et al. (2011).

first and each field is then discretized separately; this often leads to nonmatched meshes, as typical of fluid-structure interaction (Figure 6.4), and handles those naturally.

In summary, the keywords that favor the partitioned approach are: customization, independent modeling, software reuse, and modularity. However, the partitioned approach requires careful formulation and implementation to avoid serious degradation in stability and accuracy.The hope is that a partitioned algorithm can maintain that efficiency for the coupled problem if the interaction effects can be also efficiently treated.

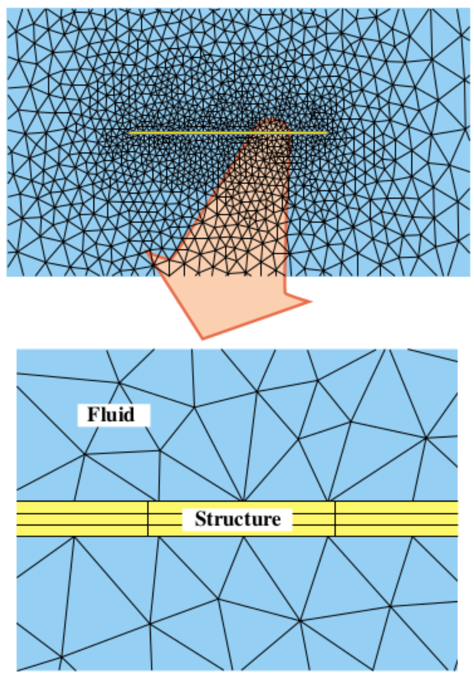

Figure 6.4. Dirrefential partitioning in two non-matching meshes for a FSI problem. Taken from Felippa et al. (2001).

APPENDIX

A. DETAILS OF TURBULENCE MODELLING

The standard $\kappa-\epsilon$ model focuses on the mechanisms that affect the turbulent kinetic energy; is based on the Boussinesq approximation with the turbulent viscosity ν_t and thermal diffusivity κ_t formulated as

$$\nu_t = C_u \frac{\kappa^2}{\epsilon} \tag{0.12}$$

$$\kappa_t = \frac{c_p \nu_t}{P_{r_t}} \tag{0.13}$$

where ϵ is the rate of dissipation of turbulence kinetic energy per unit mass due to viscous stresses. The exact ϵ-equation, contains many unknown and unmeasurable terms. The standard $\kappa - \epsilon$ model (Launder and Spalding, 1974) has two model equations, one for κ and one for ϵ. κ and ϵ are used to define velocity scale ϑ and length scale l representative of the large-scale turbulence as evidentiated on Equations 0.14 and 0.15

$$\vartheta = \kappa^{\frac{1}{2}} \tag{0.14}$$

$$l = \frac{\kappa^{\frac{3}{2}}}{\epsilon} \tag{0.15}$$

The approximation that constitutes using the 'small eddy' variable ϵ to define the 'large eddy' scale l is valid because, as explained by Versteeg and Malalasekera (1995), at high Reynolds numbers the rate at which large eddies extract energy from the mean flow is broadly matched to the rate of transfer of energy across the energy spectrum to small, dissipating, eddies if the flow does not change too rapidly. After applying a dimensional analysis, the eddy viscosity can be described as in Equation 0.16. Where C_μ is a dimensionless constant.

$$\mu_t = C\rho\vartheta l = \rho C_\mu \frac{\kappa^2}{\epsilon} \tag{0.16}$$

The standard $\kappa - \epsilon$ model uses the following transport equations for κ and ϵ, which can be describe in words, the rate of change of κ or ϵ by convection, plus the transport of κ or ϵ by diffusion equals the transport of κ or ϵ by convection, plus the rate of production of κ or

ϵ, minus the rate of destruction of κ or ϵ. Where Production and destruction of turbulent kinetic energy are always closely linked. Dissipation rate ϵ is large where production of κ is large.

The transport equations for κ and ϵ contain five adjustable constants: C_μ, σ_κ, σ_ϵ, $C1_\epsilon$ and $C2_\epsilon$ (Versteeg & Malalasekera, 1995). The standard $\kappa - \epsilon$ model employs values for the constants that are arrived at by comprehensive data fitting for a wide range of turbulent flows, and that are going to be used on this investigation as well:

$$\boxed{C_\mu = 0.09 \quad \sigma_\kappa = 1.00 \quad \sigma_\epsilon = 1.30 \quad C1_\epsilon = 1.44 \quad C2_\epsilon = 1.92}$$

For the present study the variables aforementioned were calculated in order to perform the viscous-flow computations. The turbulent intensity in all analysis was assumed 10% and the characteristic length of the turbulence was $2.17cm$, (inlet diameter of the trachea model). This resulted in $\kappa = 0.062$ and $\epsilon = 1.662452$

As explained by (Luo et al., 2004), the governing equations for LES are obtained by filtering the time-dependent Navier-Stokes equations in configuration (physical) space, (instead of time-averaging as in RANS). The process effectively filters out those eddies whose scales are smaller than the grid spacing. The resulting equations thus govern the dynamics of large eddies. This becomes sometimes necessary since, as mentioned by (Versteeg & Malalasekera, 1995), the smaller eddies are nearly isotropic and have a universal behavior (for turbulent flows at sufficiently high Re, at least); the larger eddies, on the other hand, are more anisotropic and their behavior is more problem-specific. They need to be computed with a time-dependent scheme. Therefore, LES generates an approximation to the real flow in which scales below a certain size are missing. This is corrected by having additional terms in the equation of motion, known as sub-grid terms, which only come into play at the smaller of the scales resolved by the LES.

The filtering process splits an input into a desirable part, and a rejected part. The choice of filter function determines precisely what information is retained and rejected. In finite volume implementations the filtering operation for a variable $\phi(x)$, is provided by:

$$\bar{\phi}(x) = \frac{1}{V}\int_V \phi(\prime x)G(x,\prime x)d\prime x \tag{0.17}$$

Where the reader can see from Equation 0.17 that the filtering is an integration that is carried out in three-dimensional space, as oppose as in time for the development of the RANS equations. The V is the volume of a computational cell, and the filtering function is defined as in Equation 0.18, also found in the literature as *top-hat* or *box* filter.

$$G(x, \prime x) = \begin{cases} 1 for \prime x \in V \\ 0 otherwise \end{cases} \tag{0.18}$$

Then, the filtered Navier-Stokes equations are:

$$\frac{\partial \rho}{\partial t} + div(\bar{\mathbf{u}}) = 0 \tag{0.19}$$

$$\rho \left[\frac{\partial \bar{u}}{\partial t} + div(\bar{u}\bar{\mathbf{u}}) \right] = -\frac{\partial \bar{p}}{\partial x} + \mu div(grad\bar{u}) - (div(\overline{u\mathbf{u}}) - div(\bar{u}\bar{\bar{\mathbf{u}}})) \tag{0.20}$$

$$\rho \left[\frac{\partial \bar{v}}{\partial t} + div(\bar{v}\bar{\mathbf{v}}) \right] = -\frac{\partial \bar{p}}{\partial y} + \mu div(grad\bar{v}) - (div(\overline{v\mathbf{u}}) - div(\bar{v}\bar{\mathbf{u}})) \tag{0.21}$$

$$\rho \left[\frac{\partial \bar{w}}{\partial t} + div(\bar{w}\bar{\mathbf{w}}) \right] = -\frac{\partial \bar{p}}{\partial z} + \mu div(grad\bar{w}) - (div(\overline{w\mathbf{u}}) - div(\bar{w}\bar{\mathbf{u}})) \tag{0.22}$$

Where the filtered velocity components and pressure are solved, in a very similar manner as in the RANS equations. However, the last terms found here arose as a consequence of the filtering operation and can be considered, as explained by (Versteeg & Malalasekera, 1995) as a divergence of a set of stresses. These are caused due to interactions of sub-grid scale (SGS) eddies and must be modeled. In this research, the Smagorinksy-Lilly SGS model is used.

The first subfilter-stress model, in connection with large eddy simulation, was proposed by Smagorinsky (1963) (**?**), where the length scale is chosen as grid-characteristic length scale or filter width $l = \bar{\delta} = V^{\frac{1}{3}}$. And the time scale is defined from the norm of the strain rate tensor of the resolved flow, $\bar{S} = \sqrt{2\bar{S}_{ij}\bar{S}_{ij}}$. This model recognizes the Boussinesq eddy viscosity hypothesis, where there is an intimate connection between turbulence production and mean strain, then Smagorinsky proposed that since the smallest turbulent eddies behave usually as almost isotropic, the hypothesis might accurately describe the effects of the unresolved eddies on the resolved flow. Based on this choices, the eddy viscosity is defined by Equation 0.23

$$\nu_{sgs} = (C_{SGS}\delta)^2 |\bar{S}| \tag{0.23}$$

Where, C_{SGS} is the *Smagorinsky constant*, and

$$\bar{S}_{ij} = \frac{2}{2}\left(\frac{\partial \bar{w}_i}{\partial x_j} + \frac{\partial \bar{u}_j}{\partial x_i}\right) \tag{0.24}$$

Latter on, Lilly (1967) established the following relation to calculate the constant for High Re flows as in Equation 0.25. Where the C_k is the Kolmogorov constant. However, them also suggested, based on a theoretical analysis of the decay rates of isotropic turbulent eddies in the inertial sub-range of energy spectrum, values of C_SGS between 0.17 and 0.21.

$$\frac{1}{\pi^2}\left(\frac{2}{3C_k}\right)^{\frac{3}{2}} \tag{0.25}$$

B. DETAILS OF SOLIDS4FOAM CASE SET-UP

The punch case folder found in Cardiff (2021) contains initially three folders, namely: `0`, `system` and `constant`. Additionally, two script files, `./Allrun` and `./Allclean`. In the folders the dictionary files that are to be used by OpenFOAM to perform the simulations are saved. The script files contain the instructions to run all the case-files or clean all the output from them, respectevily. This is part of the clasical OpenFOAM configuration, the aim here is to take a closer look to all of the files on this tutorial in order to understand the way solids4Foam operates. Note on Figure 0.5 there are two `.ftr` files, those correspond to the geometry files to be explained further in the text.

The OpenFOAM dictionaries are located in the `system` folder. To create a mesh in this case, the user needs to run in the command terminal the *cartesianMesh* utility, this indicates the software to go to the *meshDict* located in the `system` folder and execute the directions.

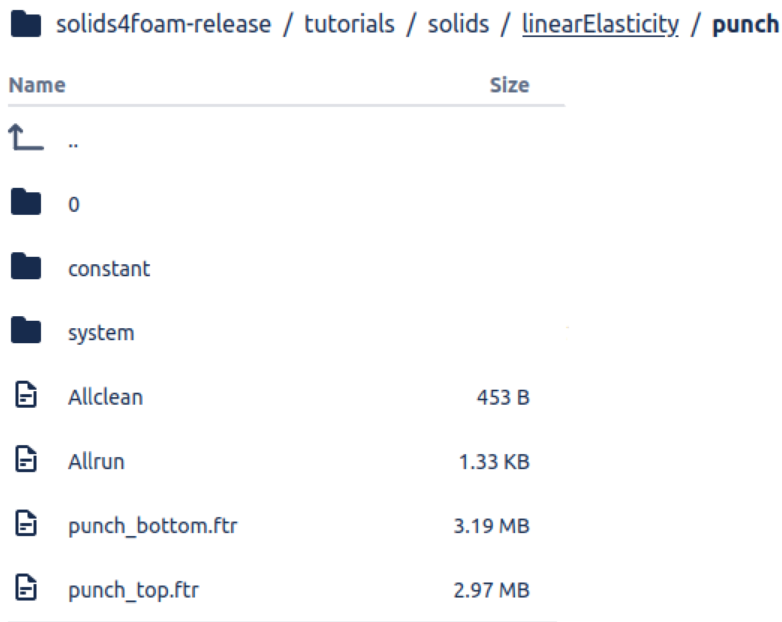

Figure 0.5. OpenFOAM case set-up for the punch case tutorial.

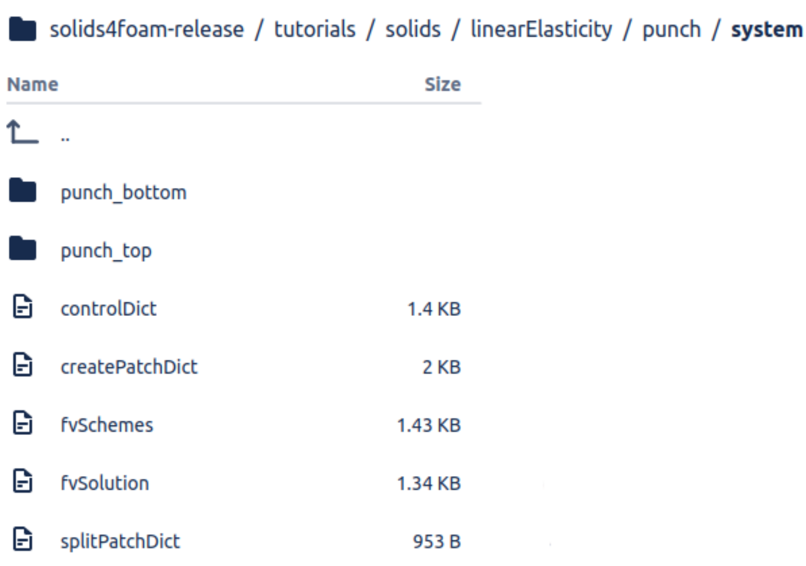

Figure 0.6. Contents of the system folder in the OpenFOAM environment.

In this case there are two additional folders in `system`, namely `punch_top` and `punch_bottom`, (see Figure 0.6), there we can find the mesh dictionaries for the puch and the cylinder geometries, respectively. Therefore, when executing the `./Allrun` command, the first order is to copy the `punch_top` mesh dictionary (`meshDict`) to the `system` folder. The meshing process is executed and the results saved in the `constant/punch_top` folder. Similar instructions appear later in the `./Allrun` script to mesh the cylinder geometry, from the `punch_bottom` folder, as seen below.

```
# Create top mesh
\cp system/punch_top/meshDict system/meshDict
runApplication -l log.cartesianMesh.punch_top cartesianMesh
mkdir constant/punch_top
\mv constant/polyMesh constant/punch_top/

# Create bottom mesh
\cp system/punch_bottom/meshDict system/meshDict
runApplication -l log.cartesianMesh.punch_bottom cartesianMesh
mkdir constant/punch_bottom
\mv constant/polyMesh constant/punch_bottom/
```

The code shown above accounts for the creation of the meshes, however, they need to be submited to other manipulations to actually simulate the problem. First, the two meshes created need to be merged as one, to do so the `mergeSubMeshsNew` utility is needed. Second, specific patches of cells have to be to splitted, this in order to apply later on the boundary conditions. Here the software uses the `createPatchDict` and `splitPatchDict`, also in the `system` folder. These can be founded in the next lines of the `./Allrun` script, as follows,

```
# Merge sub meshes
runApplication mergeSubMeshesNew punch_top punch_bottom
# Scale the geometry to metres
echo "Running transformPoints"
transformPoints -scale "(0.001 0.001 0.001)" >& log.transformPoints
# Create patches
runApplication autoPatch 45 -overwrite
runApplication createPatch -overwrite
runApplication splitPatch -overwrite
# Remove the sub meshes
\rm -rf constant/punch_top constant/punch_bottom system/meshDict
```

Now that the mesh is ready, there are some parameters that need to be specified to OpenFOAM before executing the final command. The `0` folder is used to set the initial conditions.

Here, as the study focuses on contact mechanics, the only primitive variable is the displacement vector field, and the initial conditions are contained in a "`D`" file, as shown in Figure 0.7.

```
punchLoading
{
    type            solidTraction;
    traction        uniform (0 0 0);
    pressure        uniform 100e6;
    value           uniform (0 0 0);
}
cylinderFixed
{
    type            fixedDisplacement;
    value           uniform (0 0 0);
}
punchContact
{
    type            solidContact;
    master          yes;
    rigidMaster     no;
    shadowPatch     cylinderContact;
    normalContactModel standardPenalty;
    standardPenaltyNormalModelDict
    {
        relaxationFactor 0.01;
        penaltyScale     5;
    }
    //frictionContactModel frictionless;
    frictionContactModel standardPenalty;
    standardPenaltyFrictionModelDict
    {
        relaxationFactor  0.01;
        penaltyScale      1;
        frictionLaw       coulomb;
        frictionLawDict
        {
            frictionCoeff 0.1;
        }
    }
    value           uniform (0 0 0);
}
cylinderContact
{
    type            solidContact;
    shadowPatch     punchContact;
    master          no;
    value           uniform (0 0 0);
}
punchTractionFree
{
    type            solidTraction;
    traction        uniform ( 0 0 0 );
    pressure        uniform 0;
    value           uniform (0 0 0);
}
cylinderTractionFree
{
    type            solidTraction;
    traction        uniform ( 0 0 0 );
    pressure        uniform 0;
    value           uniform (0 0 0);
}
symmx
{
    type            solidSymmetry;
    patchType       symmetryPlane;
    value           uniform (0 0 0);
}
symmy
{
    type            solidSymmetry;
    patchType       symmetryPlane;
    value           uniform (0 0 0);
}
```

Figure 0.7. Initial Boundary Conditions used for punch case in OpenFOAM environment.

We have mentioned so far the `system` and `0` folders, now, `constant` usually contains the files with parameters entered by the user needed for the model specification, (see Figure 0.8). All solids4foam cases require the `physicsProperties` dictionary; this allows the user to specify a fluid analysis, solid analysis, or fluid-solid interaction analysis.

If a solid analysis is selected in the `physicsProperties` dictionary, then solids4Foam will look for the `solidProperties` dictionary in the constant directory. This dictionary let the user specify the details of what type of solid, fluid or fluid-solid interaction analysis is to be performed. In this case, the `solidProperties` dictionary specifies the value `linearGeometryTotalDisplacement`, which means that a linear geometry mechanical approach is taken; this referrs to a "small strain" or "small strain-rotation" approach and means that the cell geometry (volumes, face areas, etc.) are assumed to be independent of the displacement field.

Figure 0.8. Constant folder contents under the OpenFOAM environment.

In all cases, we must also specify a `dynamicMeshDict`; in this case, it is set to `staticFvMesh`, which does not change the mesh during the simulation. Moreover, the gravity field `g` must be specified: here the gravity effects are neglected, therefore the value is set to zero.

A solid analysis also requires the definition of the mechanical properties via the *mechanicalProperties* dictionary; in this case the *linearElastic* law is specified.

The numerical settings are controlled with the `fvSchemes` and `fvSolution` dictionaries, located in the `system` folder. Having reviewed the case set-up in detail, the remaining line in the `./Allrun` script is: `runApplication solids4Foam`, which runs the simulation.

Now, having understood the architecture and workflow of solids contact problems in solids4Foam, some changes have to be made to tackle the idealized cuff case presented in Chapter 4. If using solely the aforedmentioned toolkit, the equivalent of `./Allrun` script for this case changes to the code below,

```
#Create background mesh
runApplication blockMesh | tee log.blockMesh

#Create cylinder mesh
cp -ar system/Cylinder/snappyHexMeshDict system/
snappyHexMesh -overwrite | tee log.snappyHexMesh.Cylinder
mkdir constant/Cylinder
mv constant/polyMesh constant/Cylinder

#Create sphere mesh
cp -ar system/Sphere/snappyHexMeshDict system/
blockMesh
snappyHexMesh -overwrite | tee log.snappyHexMesh.Sphere
mkdir constant/Sphere
mv constant/polyMesh constant/Sphere

# Merge sub meshes
runApplication mergeSubMeshesNew  Cylinder Sphere | tee log.mergeSubMeshesNew

#Create patches
runApplication autoPatch 75 -overwrite | tee log.autoPatch
runApplication createPatch -overwrite | tee log.createPatch

# Remove the sub meshes
\rm -rf constant/Cylinder constant/Sphere system/snappyHexMesh



# Run the solver
runApplication solids4Foam
```

Which, has only changes in the mesh part of it, since, as explained quite explicitly on Chapters 3 and Chapter 4, the author has predilection for the blockMesh-snappyHexMesh utilities for spatial discretization. However, following the previous script procedure arose a not-so-easy-to-work-with mesh; the reason for that is that the cylinder geometry used has very sharp edges towards what was called the inlet and outlet patches. You see, there are slight differences between OpenFoam versions, and the `snappyHexMeshDict` in OpenFoam-extended

4.0, (which is the one solids4Foam compiles with), does not support for edge refinement, only surfaces, whereas the standard OpenFOAM V8 does. Having that in mind, when executing the `autoPatch` utility, many different patches were created since the cells around the edges was not refined enough. Resulting in a mesh were no initial conditions could be set.

In that sense, the alternative option, if the reader find themselves working with that type of geometry is to do the meshing in the standard version of OpenFOAM, and then simulate the case in the extended project with solids4Foam. In order to do so, the process would be as next shown,

```
#Create background mesh
blockMesh | tee log.blockMesh

#Extract surfaces
surfaceFeatures

#Create cylinder mesh
cp -ar system/Cylinder/snappyHexMeshDict system/
snappyHexMesh -overwrite | tee log.snappyHexMesh.Cylinder
mv constant/polyMesh constant/Cylinder

#Create sphere mesh
cp -ar system/Sphere/snappyHexMeshDict system/
blockMesh
snappyHexMesh -overwrite | tee log.snappyHexMesh.Sphere
mv constant/polyMesh constant/Sphere

# Merge sub meshes
mergeMeshes Cylinder/ Sphere/ | tee log.mergeMeshes

#Create patches
autoPatch 75 -overwrite | tee log.autoPatch
createPatch -overwrite | tee log.createPatch

# Remove the sub meshes
\rm -rf constant/Cylinder constant/Sphere system/Cylinder system/Sphere

# Create cellZones
topoSet | tee log.topoSet

# Make the mesh compatible with the OpenFOAM-extended 4.0 version.
compactFaceToFace
```

Where the reader can appreciate new commands, to give some brief description of them, the `surfaceFeatures` reads the .STL geometry in the `constant/triSurface` folder, extracts the edges from it and writes them in a .eMesh file that latter is used in `snappyHexMeshDict` to refine those sharp edges, given a much more desirable mesh. Note also that `mergeMeshes`, is a different command, instead of `mergeSubMeshesNew` seen before but with the same function.

When meshing in the extended project the `constant/polyMesh/cellZones` file is created with the zones that the user later uses to specify the mechanical properties,for example, in the punch case the mechanical properties were set to just two zones (`punch_top` and `punch_bottom`), regardless of the patches that were seven. In the cuff case there are six patches to impose IC, but the mechanical properties are only set to the cylinder, and the sphere. Problem is, when meshing in the standard version, that file (`constant/polyMesh/cellZones`) is empty, which is why to use the `topoSet` utility.

The `compactFaceToFace` command at the end is used since the generated file `constant/polyMesh/faces` has also differences between versions, to deal with that the user needs to download from Bachant (2021) the code of the utility and built in the standard OpenFOAM environment. Once executed those commands, the simulation folder can be copied to run under the solids4Foam toolkit. Finally, there are also differences between the parallel computations between versions, that is why the author chose to run in series, since it is a small geometry that does not really take a lot of time to mesh; the reader however is encouraged to try that option if the situation calls for it.

As a final remark to the conscious reader: it becomes evident that simulating in open-source software has many advantages but also requires patient and stubborn users willing to read every forum and copy every tutorial in order to make their case work. On that note, don't worry, if you got to this point, you are probably curious enough to enroll in the open-source simulations endeavor, and for your patience, I thank you.

References

Ahmadi, J. T. K. I. G. (2013). *Computational fluid and particle dynamics in the human respiratory system* (S. S. M. Dordrecht, Ed.). Springer Netherlands. doi: 10.1007/978-94-007-4488-2

Bachant, P. (2021, August). *compactfacetoface.* Retrieved from https://github.com/petebachant/compactFaceToFace

Bathe, K.-J., Hou Zhang, & Ji, S. (1999). Finite element analysis of fluid flows fully coupled with structural interactions. *Computers & Structures*, *72*(1), 1 - 16. Retrieved from http://www.sciencedirect.com/science/article/pii/S0045794999000425 doi: https://doi.org/10.1016/S0045-7949(99)00042-5

Bathe, K.-J., & Zhang, H. (2004). Finite element developments for general fluid flows with structural interactions. *International Journal for Numerical Methods in Engineering*, *60*(1), 213-232. Retrieved from https://onlinelibrary.wiley.com/doi/abs/10.1002/nme.959 doi: 10.1002/nme.959

Bhalla, A. P. S., Bale, R., Griffith, B. E., & Patankar, N. A. (2013, October). A unified mathematical framework and an adaptive numerical method for fluid-structure interaction with rigid, deforming, and elastic bodies. *Journal of Computational Physics*, *250*, 446–476. Retrieved from http://www.sciencedirect.com/science/article/pii/S0021999113003173

Blot, S. I., Poelaert, J., & Kollef, M. (2014, November). How to avoid microaspiration? a key element for the prevention of ventilator-associated pneumonia in intubated icu patients. *BMC Infectious Diseases*, *14*(1), 119. Retrieved from https://doi.org/10.1186/1471-2334-14-119

Blot, S. I., Rello, J., & Koulenti, D. (2016, Jun). The value of polyurethane-cuffed endotracheal tubes to reduce microaspiration and intubation-related pneumonia: a systematic review of laboratory and clinical studies. *Critical care (London, England)*, *20*, 203.

Calay, R., Kurujareon, J., & Holdø, A. E. (2002). Numerical simulation of respiratory flow patterns within human lung. *Respiratory Physiology & Neurobiology*, *130*(2), 201 - 221. Retrieved from http://www.sciencedirect.com/science/article/pii/S0034568701003371 doi: https://doi.org/10.1016/S0034-5687(01)00337-1

Cardiff, P. (2021, Jun). *solids4foam - a finite volume toolbox for solid mechanics and fluid solid interaction simulations.* Retrieved from https://bitbucket.org/philip_cardiff/solids4foam-release/src/master/tutorials/solids/linearElasticity/punch/

Cardiff, P., Karac, A., & Ivankovic, A. (2014, March). Development of a finite volume contact solver based on the penalty method. *Computational Materials Science*, *64*, 283-284. doi: 10.1016/j.commatsci.2012.03.011

Cardiff, P., Karač, A., Jaeger, P. D., Jasak, H., Nagy, J., Ivanković, A., & Tuković, Ž. (2018). *An open-source finite volume toolbox for solid mechanics and fluid-solid interaction simulations.*

Chan, T. L., & Lippmann, M. (1980, Jun). Experimental measurements and empirical modelling of the regional deposition of inhaled particles in humans. *American Industrial Hygiene Association journal*, *41*, 399-409.

Cui, X. (2012). *Cfd study of the flow field and particle dispersion and deposition in the upper human respiratory system* (Doctoral dissertation, Ruperto-Carola University of Heidelberg). doi: https://doi.org/10.11588/heidok.00013457

Cui, X., & Gutheil, E. (2017). Three-dimensional unsteady large eddy simulation of the vortex structures and the mono-disperse particle dispersion in the idealized human upper respiratory system. *Journal of Aerosol Science*, *114*, 195 - 208. Retrieved from http://www.sciencedirect.com/science/article/pii/S0021850217300186 doi: https://doi.org/10.1016/j.jaerosci.2017.09.005

Cui, X., Wu, W., & Gutheil, E. (2018). Numerical study of the airflow structures in an idealized mouth-throat under light and heavy breathing intensities using large eddy simulation. *Respiratory Physiology & Neurobiology*, *248*, 1 - 9. Retrieved from http://www.sciencedirect.com/science/article/pii/S1569904817303075 doi: https://doi.org/10.1016/j.resp.2017.11.001

Dailey, H., & Ghadiali, S. (2007). Fluid-structure analysis of microparticle transport in deformable pulmonary alveoli. *Journal of Aerosol Science*, *38*(3), 269 - 288. Retrieved from http://www.sciencedirect.com/science/article/pii/S0021850207000183 doi: https://doi.org/10.1016/j.jaerosci.2007.01.001

Dave, M. H., Frotzler, A., & Weiss, M. (2011, Feb). Closed tracheal suction and fluid aspiration past the tracheal tube. impact of tube cuff and airway pressure. *Minerva anestesiologica*, *77*, 166-71.

Deng, Q., Ou, C., Shen, Y.-M., Xiang, Y., Miao, Y., & Li, Y. (2019, March). Health effects of physical activity as predicted by particle deposition in the human respiratory tract. *Science of The Total Environment*, *657*, 819–826. Retrieved from http://www.sciencedirect.com/science/article/pii/S0048969718349076

Donea, J., Huerta, A., Ponthot, J.-P., & Rodriguez-Ferran, A. (2004, November). Arbitrary lagrangian-eulerian methods. In (Vol. 1, pp. 413–437). doi: 10.1002/0470091355.ecm009

Doorly, D., Taylor, D., & Schroter, R. (2008). Mechanics of airflow in the human nasal airways. *Respiratory Physiology & Neurobiology*, *163*(1), 100 - 110. Retrieved from http://www.sciencedirect.com/science/article/pii/S1569904808002140 (Respiratory Biomechanics) doi: https://doi.org/10.1016/j.resp.2008.07.027

Esteban, A., Frutos-Vivar, F., Muriel, A., Ferguson, N. D., Peñuelas, O., Abraira, V., ... Anzueto, A. (2013, Jul). Evolution of mortality over time in patients receiving mechanical ventilation. *American journal of respiratory and critical care medicine*, *188*, 220-30.

Faizal, W., Ghazali, N., Khor, C., Badruddin, I. A., Zainon, M., Yazid, A. A., ... Razi, R. M. (2020). Computational fluid dynamics modelling of human upper airway: A review. *Computer Methods and Programs in Biomedicine*, *196*, 105627. Retrieved from http://www.sciencedirect.com/science/article/pii/S0169260720314607 doi: https://doi.org/10.1016/j.cmpb.2020.105627

Felippa, C., Park, K. C., & Farhat, C. (2001, March). Partitioned analysis of coupled system. *Computer Methods in Applied Mechanics and Engineering*, *190*, 3247-3270. doi: 10.1016/S0045-7825(00)00391-1

Fernandez, J. F., Levine, S. M., & Restrepo, M. I. (2012, Jul). Technologic advances in endotracheal tubes for prevention of ventilator-associated pneumonia. *Chest*, *142*, 231-238.

Ghahramani, E., Abouali, O., Emdad, H., & Ahmadi, G. (2017). Numerical investigation of turbulent airflow and microparticle deposition in a realistic model of human upper airway using les. *Computers & Fluids*, *157*, 43 - 54. Retrieved from http://www.sciencedirect.com/science/article/pii/S0045793017302748 doi: https://doi.org/10.1016/j.compfluid.2017.08.003

Greenshields, C. (2018, July). *Openfoam v6 user guide: 5.4 mesh generation with snappyhexmesh.* Retrieved from https://cfd.direct/openfoam/user-guide/v6-snappyhexmesh/

Guerrero, J. (2019, August). *Crash introduction to the fvm and numerical playground.* CC BY-SA license. Retrieved from http://www.wolfdynamics.com/wiki/fvm_crash_intro.pdf

Guidelines for the management of adults with hospital-acquired, ventilator-associated, and healthcare-associated pneumonia. (2005, Feb). *American journal of respiratory and critical care medicine*, *171*, 388-416.

Hans-Joachim Bungartz, M. S., Miriam Mehl (Ed.). (2010). *Fluid structure interaction ii. modelling, simulation, optimization.* (Vol. 73) (No. 1). Springer-Verlag Berlin Heidelberg. doi: 10.1007/978-3-642-14206-2

Huang, J., & Zhang, L. (2011). Numerical simulation of micro-particle deposition in a realistic human upper respiratory tract model during transient breathing cycle. *Particuology*, *9*(4), 424 - 431. Retrieved from http://www.sciencedirect.com/science/article/pii/S1674200111000666 (Multiscale Modeling and Simulation of Complex Particulate Systems) doi: https://doi.org/10.1016/j.partic.2011.02.004

Jaillette, E., Girault, C., Brunin, G., Zerimech, F., Behal, H., Chiche, A., ... Nseir, S. (2017, Nov). Impact of tapered-cuff tracheal tube on microaspiration of gastric contents in intubated critically ill patients: a multicenter cluster-randomized cross-over controlled trial. *Intensive care medicine*, *43*, 1562-1571.

Karaman, R., & Tsega, E. G. (2018, October). Computational fluid dynamics modeling of respiratory airflow in tracheobronchial airways of infant, child, and adult. *Computational and Mathematical Methods in Medicine*, *2018*, 9603451. Retrieved from https://doi.org/10.1155/2018/9603451

Kim, Y., Tong, Z., Chan, H., & Yang, R. (2019). Cfd modelling of air and particle flows in different airway models. *Journal of Aerosol Science*, *134*, 14 - 28. Retrieved from http://www.sciencedirect.com/science/article/pii/S0021850218301435 doi: https://doi.org/10.1016/j.jaerosci.2019.04.015

Li Bassi, G., Luque, N., MartÃ, J. D., Aguilera Xiol, E., Di Pasquale, M., Giunta, V., ... Torres, A. (2015, May). Endotracheal tubes for critically ill patients: an in vivo analysis of associated tracheal injury, mucociliary clearance, and sealing efficacy. *Chest*, *147*, 1327-1335.

Liu, Y., Mitchell, J., Chen, Y., Yim, W., Chu, W., & Wang, R. C. (2018). Study of the upper airway of obstructive sleep apnea patient using fluid structure interaction. *Respiratory Physiology and Neurobiology*, *249*, 54-61. Retrieved from https://www.sciencedirect.com/science/article/pii/S1569904817303865 doi: 10.1016/j.resp.2018.01.005

Lizal, F., Jedelsky, J., Morgan, K., Bauer, K., Llop, J., Cossio, U., ... Schnabel, C. (2018). Experimental methods for flow and aerosol measurements in human airways and their replicas. *European Journal of Pharmaceutical Sciences*, *113*, 95 - 131. Retrieved from http://www.sciencedirect.com/science/article/pii/S0928098717304657 (A special issue dedicated to COST Action SimInhale: cross-disciplinary perspective on the current state of the art and challenges in pulmonary drug delivery) doi: https://doi.org/10.1016/j.ejps.2017.08.021

Lorente, L., Lecuona, M., JimÃ©nez, A., Mora, M. L., & Sierra, A. (2007, Dec). Influence of an endotracheal tube with polyurethane cuff and subglottic secretion drainage on pneumonia. *American journal of respiratory and critical care medicine*, *176*, 1079-83.

Lorenzo, R. (2016). *Implementation and application of the actuator line model by openfoam for a vertical axis wind turbine set on a university of stavanger building roof.* (Unpublished master's thesis). POLITECNICO DI MILANO.

Luca Formaggia, A. V., Alfio Quarteroni. (2009). *Cardiovascular mathematics. modeling and simulation of the circulatory system.* (Vol. 1; A. V. Luca Formaggia Alfio Quarteroni, Ed.). Springer-Verlag Mailand. doi: 10.1007/978-88-470-1152-6

Luo, X., Hinton, J., Liew, T., & Tan, K. (2004). Les modelling of flow in a simple airway model. *Medical Engineering & Physics*, *26*(5), 403 - 413. Retrieved from http://www.sciencedirect.com/science/article/pii/S1350453304000347 doi: https://doi.org/

10.1016/j.medengphy.2004.02.008

Malvè, M., del Palomar, A. P., López-Villalobos, J. L., Ginel, A., & Doblaré, M. (2010, Apr). Fsi analysis of the coughing mechanism in a human trachea. *Annals of biomedical engineering*, *38*, 1556-65.

Malvè, M., Pérez del Palomar, A., Trabelsi, O., Lṕez-Villalobos, J., Ginel, A., & Doblaré, M. (2011). Modeling of the fluid structure interaction of a human trachea under different ventilation conditions. *International Communications in Heat and Mass Transfer*, *38*(1), 10 - 15. Retrieved from http://www.sciencedirect.com/science/article/pii/S0735193310002393 doi: https://doi.org/10.1016/j.icheatmasstransfer.2010.09.010

Margolin, L. (1997, August). Introduction to 'an arbitrary lagrangian eulerian computing method for all flow speeds'. *Journal of Computational Physics*, *135*, 198–202. doi: 10.1006/jcph.1997.5727

Maury, B. (2013). *The respiratory system in equations* (1st ed., Vol. 7). Springer-Verlag Mailand. Retrieved from https://www.springer.com/gp/book/9788847052130 doi: 10.1007/978-88-470-5214-7

Moukalled, F., Mangani, L., & Darwish, M. (2015). *The finite volume method in computational fluid dynamics: An advanced introduction with openfoam and matlab* (Vol. 113). doi: 10.1007/978-3-319-16874-6

Muscedere, J., Rewa, O., McKechnie, K., Jiang, X., Laporta, D., & Heyland, D. K. (2011, Aug). Subglottic secretion drainage for the prevention of ventilator-associated pneumonia: a systematic review and meta-analysis. *Critical care medicine*, *39*, 1985-91.

Mylavarapu, G., Murugappan, S., Mihaescu, M., Kalra, M., Khosla, S., & Gutmark, E. (2009). Validation of computational fluid dynamics methodology used for human upper airway flow simulations. *Journal of Biomechanics*, *42*(10), 1553 - 1559. Retrieved from http://www.sciencedirect.com/science/article/pii/S0021929009001341 doi: https://doi.org/10.1016/j.jbiomech.2009.03.035

Nair, G. B., & Niederman, M. S. (2015, Jan). Ventilator-associated pneumonia: present understanding and ongoing debates. *Intensive care medicine*, *41*, 34-48.

Necasová, T. B. G. P. G. S. (Ed.). (2014). *Fluid structure interaction and biomedical applications* (1st ed.). Birkhauser Basel. doi: 10.1007/978-3-0348-0822-4

Papazian, L., Klompas, M., & Luyt, C.-E. (2020, May). Ventilator-associated pneumonia in adults: a narrative review. *Intensive care medicine*, *46*, 888-906.

Park, J.-H., Koh, H. M., & Kim, J. (1992). Fluid-structure interaction analysis by a coupled boundary element-finite element method in time domain. In C. A. Brebbia & M. S. Ingber (Eds.), *Boundary element technology vii* (pp. 227–243). Dordrecht: Springer Netherlands. Retrieved from https://doi.org/10.1007/978-94-011-2872-8_16

Paz, C., SuÁrez, E., Concheiro, M., & Porteiro, J. (2017, 05). Cfd transient simulation of a breathing cycle in an oral-nasal extrathoracic model. *Journal of Applied Fluid Mechanics*, *10*, 777-784. doi: 10.18869/acadpub.jafm.73.240.25348

Philippart, F., Gaudry, S., Quinquis, L., Lau, N., Ouanes, I., Touati, S., ... Misset, B. (2015, Mar). Randomized intubation with polyurethane or conical cuffs to prevent pneumonia in ventilated patients. *American journal of respiratory and critical care medicine*, *191*, 637-45.

Phuong, N. L., & Ito, K. (2015). Investigation of flow pattern in upper human airway including oral and nasal inhalation by piv and cfd. *Building and Environment*, *94*, 504 - 515. Retrieved from http://www.sciencedirect.com/science/article/pii/S0360132315301414 doi: https://doi.org/10.1016/j.buildenv.2015.10.002

Pneumatikos, I., Dragoumanis, C., Bouros, D., Warner, D., & Warner, M. (2009, 03). Ventilator-associated Pneumonia or Endotracheal Tube-associated Pneumonia?: An Approach to the Pathogenesis and Preventive Strategies Emphasizing the Importance of Endotracheal Tube. *Anesthesiology*, *110*(3), 673-680. Retrieved from https://doi.org/10.1097/ALN.0b013e31819868e0 doi: 10.1097/ALN.0b013e31819868e0

Rahimi-Gorji, M., Pourmehran, O., Gorji-Bandpy, M., & Gorji, T. (2015, September). Cfd simulation of airflow behavior and particle transport and deposition in different breathing conditions through the realistic model of human airways. *Journal of Molecular Liquids*, *209*.

Rasani, M., Inthavong, K., & Tu, J. Y. (2011, March). Simulation of pharyngeal airway interaction with air flow using low-re turbulence model. *Modelling and Simulation in Engineering*, *2011*, 1–9. doi: 10.1155/2011/510472

Richter, T. (2010, 08). Numerical methods for fluid-structure interaction problems.

Richter, T. (2017). *Fluid structure interactions: Models, analysis and finite elements.* (S. I. P. AG, Ed.). Springer International Publishing. doi: 10.1007/978-3-319-63970-3

Rosero, E. B., Ozayar, E., Eslava Schmalbach, J., Minhajuddin, A., & Joshi, G. P. (2018, July). Effects of increasing airway pressures on the pressure of the endotracheal tube cuff during pelvic laparoscopic surgery. *Anesthesia and analgesia*, *127*(1), 120-125. doi: 10.1213/ane.0000000000002657

RouzÃ©, A., Jaillette, E., Poissy, J., PrÃ©au, S., & Nseir, S. (2017, Oct). Tracheal tube design and ventilator-associated pneumonia. *Respiratory care*, *62*, 1316-1323.

Shang, Y., Dong, J., Tian, L., Inthavong, K., & Tu, J. (2020, November). Detailed computational analysis of flow dynamics in an extended respiratory airway model. *Clinical Biomechanics*, *61*, 105–111. Retrieved from https://doi.org/10.1016/j.clinbiomech.2018.12.006 doi: 10.1016/j.clinbiomech.2018.12.006

Spapen, H. D., Suys, E., Diltoer, M., Stiers, W., Desmet, G., & HonorÃ©, P. M. (2017, Jul). A newly developed tracheal tube offering 'pressurised sealing' outperforms currently available tubes in preventing cuff leakage: A benchtop study. *European journal of anaesthesiology*, *34*, 411-416.

Srivastav, V., Paul, A., & Jain, A. (2012, 12). Cfd simulation of airflow and particle deposition in third to sixth generation human respiratory tract..

Srivastav, V. K., Paul, A. R., & Jain, A. (2019). Capturing the wall turbulence in cfd simulation of human respiratory tract. *Mathematics and Computers in Simulation*, *160*, 23 - 38. Retrieved from http://www.sciencedirect.com/science/article/pii/S0378475418303148 doi: https://doi.org/10.1016/j.matcom.2018.11.019

Suhas, P., Kundra, P., & Cherian, A. (2016, Mar). Polyurethane cuffed versus conventional endotracheal tubes: Effect on ventilator-associated pneumonia rates and length of intensive care unit stay. *Indian journal of anaesthesia*, *60*, 163-7.

Trabelsi, O., del Palomar, A. P., López-villalobos, J. L., Ginel, A., & Doblaré, M. (2010). Experimental characterization and constitutive modeling of the mechanical behavior of the human trachea. *Medical Engineering and Physics*, *32*(1), 76-82. Retrieved from https://www.sciencedirect.com/science/article/pii/S1350453309002161 doi: 10.1016/j.medengphy.2009.10.010

Vaish, M. (2014). *Lung-aerosol dynamics in human airway models: Validation and application of openfoam software* (Master's thesis, North Carolina State University). Retrieved from https://repository.lib.ncsu.edu/bitstream/handle/1840.16/9752/etd.pdf?sequence=2

Vaish, M., Kleinstreuer, C., Kolanjiyil, A., Saini, N., & Pillalamarri, N. (2016, 01). Laminar/turbulent airflow and microsphere deposition in a patient-specific airway geometry using an open-source solver. *International Journal of Biomedical Engineering and Technology*, *22*, 145. doi: 10.1504/IJBET.2016.079145

Valencia, M., Ferrer, M., Farre, R., Navajas, D., Badia, J. R., Nicolas, J. M., & Torres, A. (2007, Jun). Automatic control of tracheal tube cuff pressure in ventilated patients in semirecumbent position: a randomized trial. *Critical care medicine*, *35*, 1543-9.

Versteeg, H., & Malalasekera, H. (1995, 01). An introduction to computational fluid dynamics. *Essex, England: Prentice Hall - Pearson Education Limited*.

Wall, W. A., & Rabczuk, T. (2008). Fluid structure interaction in lower airways of ct based lung geometries. *International Journal for Numerical Methods in Fluids*, *57*(5), 653-675. Retrieved from https://onlinelibrary.wiley.com/doi/abs/10.1002/fld.1763 doi: 10.1002/fld.1763

Weiss, M., Doell, C., Koepfer, N., Madjdpour, C., Woitzek, K., & Bernet, V. (2009, Feb). Rapid pressure compensation by automated cuff pressure controllers worsens sealing in tracheal tubes. *British journal of anaesthesia*, *102*, 273-8.

Xu, X., Wu, J., Weng, W., & Fu, M. (2020, 02). Investigation of inhalation and exhalation flow pattern in a realistic human upper airway model by piv experiments and cfd simulations. *Biomechanics and Modeling in Mechanobiology*, *19*. doi: 10.1007/s10237-020-01299-3

Xu, X. Y., Ni, S. J., Fu, M., Zheng, X., Luo, N., & Weng, W. G. (2017, December). Numerical investigation of airflow, heat transfer and particle deposition for oral breathing in a realistic human upper airway model. *Journal of Thermal Biology*, *70*, 53–63. Retrieved from http://

www.sciencedirect.com/science/article/pii/S0306456516304387

Zhang, Z., & Kleinstreuer, C. (2011). Computational analysis of airflow and nanoparticle deposition in a combined nasal oral tracheobronchial airway model. *Journal of Aerosol Science*, *42*(3), 174 - 194. Retrieved from http://www.sciencedirect.com/science/article/pii/S0021850211000097 doi: https://doi.org/10.1016/j.jaerosci.2011.01.001